AD-A096 048 ATLANTIC RESEARCH CORP ALEXANDRIA VA F/G 20/4
IMPROVED BODIES OF REVOLUTION.(U)
JAN 81 H K SCHUMAN F30602-80-C-0087
UNCLASSIFIED RADC-TR-80-389 NL

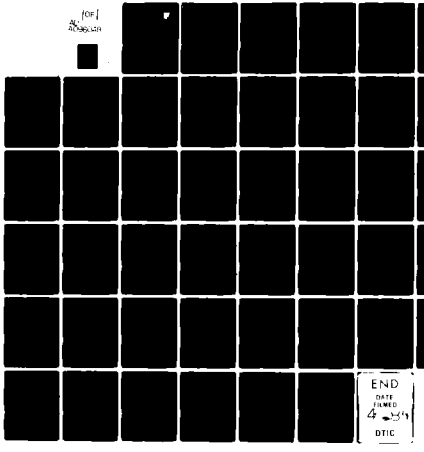

RADC-TR-80-389
Final Technical Report
January 1981

IMPROVED BODIES OF REVOLUTION

Atlantic Research Corporation

H.K. Schuman

ROME AIR DEVELOPMENT CENTER
Air Force Systems Command
Griffiss Air Force Base, New York 13441

This report has been reviewed by the RADC Public Affairs Office (PA) and is releasable to the National Technical Information Service (NTIS). At NTIS it will be releasable to the general public, including foreign nations.

RADC-TR-80-389 has been reviewed and is approved for publication.

APPROVED: Daniel E. Warren

DANIEL E. WARREN
Project Engineer

APPROVED: David C. Luke

DAVID C. LUKE, Colonel, USAF
Chief, Reliability & Compatibility Division

FOR THE COMMANDER: John P. Huss

JOHN P. HUSS
Acting Chief, Plans Office

If your address has changed or if you wish to be removed from the RADC mailing list, or if the addressee is no longer employed by your organization, please notify RADC (RBCT), Griffiss AFB NY 13441. This will assist us in maintaining a current mailing list.

Do not return this copy. Retain or destroy.

MISSION
of
Rome Air Development Center

RADC plans and executes research, development, test and selected acquisition programs in support of Command, Control Communications and Intelligence (C^3I) activities. Technical and engineering support within areas of technical competence is provided to ESD Program Offices (POs) and other ESD elements. The principal technical mission areas are communications, electromagnetic guidance and control, surveillance of ground and aerospace objects, intelligence data collection and handling, information system technology, ionospheric propagation, solid state sciences, microwave physics and electronic reliability, maintainability and compatibility.

UNCLASSIFIED

SECURITY CLASSIFICATION OF THIS PAGE (When Data Entered)

19 REPORT DOCUMENTATION PAGE		READ INSTRUCTIONS BEFORE COMPLETING FORM
1. REPORT NUMBER RADC-TR-80-389	2. GOVT ACCESSION NO. AD-A096 048	3. RECIPIENT'S CATALOG NUMBER
4. TITLE (and Subtitle) IMPROVED BODIES OF REVOLUTION.		5. TYPE OF REPORT & PERIOD COVERED Final Technical Report. 26 Feb 80 - 26 May 80.
		6. PERFORMING ORG. REPORT NUMBER N/A
7. AUTHOR(s) H.K. Schuman		8. CONTRACT OR GRANT NUMBER(s) F30602-80-C-0087
9. PERFORMING ORGANIZATION NAME AND ADDRESS Atlantic Research Corporation 5390 Cherokee Avenue Alexandria VA 22314		10. PROGRAM ELEMENT, PROJECT, TASK AREA & WORK UNIT NUMBERS 64747F 20640310 1703
11. CONTROLLING OFFICE NAME AND ADDRESS Rome Air Development Center (RBCT) Griffiss AFB NY 13441		12. REPORT DATE January 1981 13. NUMBER OF PAGES 74
14. MONITORING AGENCY NAME & ADDRESS(if different from Controlling Office) Same		15. SECURITY CLASS. (of this report) UNCLASSIFIED 15a. DECLASSIFICATION DOWNGRADING SCHEDULE N/A

16. DISTRIBUTION STATEMENT (of this Report)

Approved for public release; distribution unlimited

17. DISTRIBUTION STATEMENT (of the abstract entered in Block 20, if different from Report)

Same

18. SUPPLEMENTARY NOTES

RADC Project Engineer: Daniel E. Warren (RBCT)

19. KEY WORDS (Continue on reverse side if necessary and identify by block number)

Aperture Coupling
Bodies of Revolution
Method of Moments
Electromagnetic Coupling
Near Field Computation
Electromagnetic Fields Analysis

20. ABSTRACT (Continue on reverse side if necessary and identify by block number)

The aperture loading technique (ALT) is implemented in an aperture coupling body of revolution (BOR) computer code. Apertures of material fill (dielectric, composite, conductive putty, etc.) are amenable to ALT analysis. Thin apertures formed from complex shaped walls, e.g., sleeve-fit seams, also are amenable to ALT analysis. The ALT BOR code is applied to a plane wave excited, missile shaped BOR with a dielectric filled sleeve-fit seam. Interior E-fields and H-fields are mapped.

DD FORM 1 JAN 73 1473 EDITION OF 1 NOV 65 IS OBSOLETE

UNCLASSIFIED 045550

SECURITY CLASSIFICATION OF THIS PAGE (When Data Entered)

TABLE OF CONTENTS

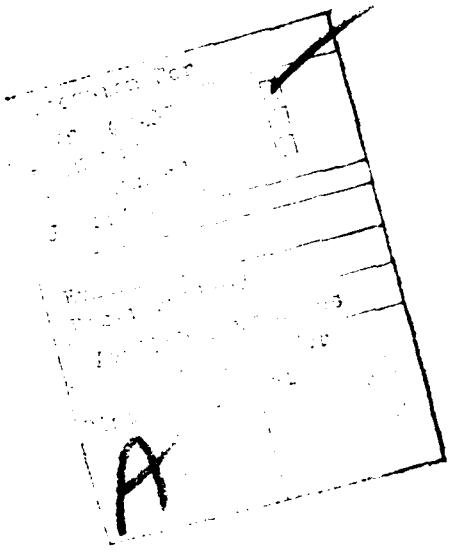

LIST OF ILLUSTRATIONS

EVALUATION

The purpose of this effort was to demonstrate the concept of Equivalent Aperture Loading (EAL) and interface this concept with the "Method of Moments" (MOM) analysis called "Bodies of Revolution" (BOR). The reason that this combination was chosen is that previously MOM and BOR were applied to a conceptual aperture coupling problem on board a missile. The results were found to be questionable because of the inability to accurately model the complex shaped aperture involved. This effort combined the EAL technique with MOM in an attempt to correct this deficiency and at the same time demonstrate that such a hybridization of techniques is cost effective in terms of computer resources.

The results of the field mapping inside the missile are contained in this report and will be compared to those obtained from measured data associated with another RADC/RBCT project when it is completed.

The advantage of this technology are a computer cost savings by hybridizing two or more analysis techniques while maintaining a reasonable degree of accuracy.

Daniel E. Warren

DANIEL E. WARREN
Project Engineer

SECTION I

INTRODUCTION

Bodies of revolution (BORs) are rotationally symmetric structures that approximate the enclosures of many practical systems such as missiles and aircraft fuselages. The aperture loading technique (ALT) is applied here to predict the plane wave excited E- and H-fields penetrating a thin, conducting walled BOR. The BOR has an open front end and a thin, dielectric-filled, sleeve-fit seam formed by overlapping walls. The present version of the computer code implementing ALT applies to arbitrarily shaped BORs with any number of simple apertures (circumferential wall separations) and one thin capacitive seam. The code can apply, with minor modification, to any number of odd-shaped seams and openings with material fill; e.g., conductive putty, fiber glass, or composite.

The aperture characteristics are dealt with naturally in a localized manner. In the case of composites, this permits relative ease in accounting for the anisotrophy of the medium. The aperture characteristics can be varied for reasonably small apertures with only minor changes in computation. This is particularly useful for apertures that are ill-defined where only an average response or other statistical measure is appropriate. An ill-defined aperture, for example, is a sleeve-fit seam in a missile shell; the spacing between seam walls may vary from missile to missile since the fit is designed to be as "tight" as possible. Several examples of such apertures are shown in Figure 1.

The computer code extends the capability of an earlier BOR aperture coupling code, BOR3 [9], principally by employing ALT. Additional extensions and improvements include near H-field computation, ϕ- as well as θ-polarized plane wave excitation, computer memory requirement reduction by approximately 60 percent, and out-of-core matrix computation and inversion. The out-of-core capability allows large problems to be solved if long run times can be tolerated. The present version of the code [4] is a collection of several codes and is operational on a PDP-11/34 minicomputer. The solutions presented in this report were obtained with the PDP-11/34.

As with BOR3, the ALT BOR code is based on a Harrington/Mautz BOR moment method for obtaining plane wave excited scattering currents. The Harrington/Mautz code employed in developing the ALT BOR code is a revision of the original Harrington/Mautz code [12] employed in BOR3. The revised Harrington/Mautz code [1] sacrifices some accuracy in matrix element computation but achieves at least 50 percent faster run time. The revision, however, is applicable only to closed bodies; therefore an

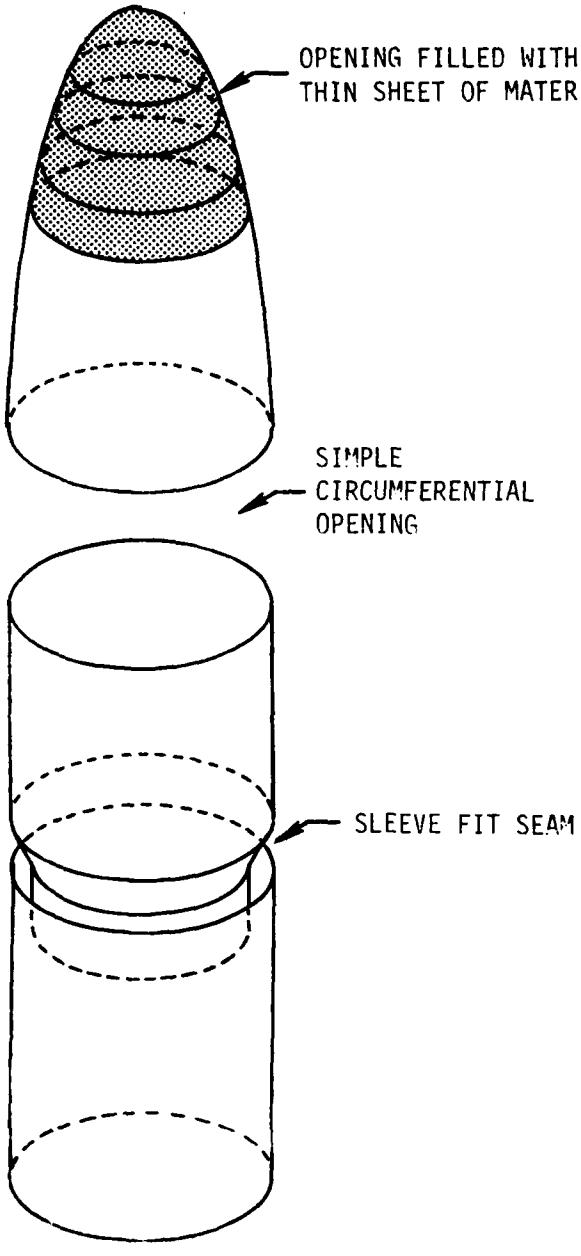

Figure 1. Body of Revolution with Several Types of Apertures

edge element expansion function was incorporated in the ALT BOR code in the same manner as in the original Harrington/Mautz code.

It also was necessary to alter the near E-field computation from that of BOR3; however, it still follows closely Bevensee's approach [6] as employed in BOR3. A near H-field computation also was included. The theory and coding were adapted from a Harrington/Mautz H-field formulation BOR moment method [11].

A third Harrington/Mautz E-field formulation moment method BOR scattering code has recently become available [13]. This code is superior to the previous Harrington/Mautz codes, especially in the manner in which it treats edge effects. Following the work of Wilton and Glission [10], they employed a "shifted" pulse type expansion function for the ϕ-directed surface current component with excellent success in removing the computationally induced surface current oscillations that occur with some geometries. An ALT BOR code based on this improved BOR code presently is under development.

The ALT BOR code also is based in part on the equivalent aperture excitation technique (EAET). The EAET is characterized by greater sensitivity over the conventional near-field scattering method [6] in that small field strengths are determined more accurately. In the conventional method, the surface current induced on the conducting portion of the body and its corresponding scattered field are determined. The internal field then is found by adding the impressed (exciting field in the absence of the body) and scattered fields. For small field levels, such as those associated with tiny apertures, this computation involves a subtraction of almost equal numbers with a corresponding loss in accuracy. This difficulty is avoided with the EAET because the internal field is computed as a radiation problem once an equivalent aperture excitation is determined. The improvement in sensitivity of the EAET over the conventional method has been demonstrated [9].

The BOR3 code was the first to employ the EAET. The EAET subsequently has been employed in a moment method, body of translation, aperture coupling code [14]. The EAET also has been incorporated in a moment method BOR code in a more efficient manner than in BOR3 [10].

A detailed theoretical treatment of the ALT BOR code from basic BOR theory to the EAET is given in Appendix A. ALT is a natural extension of the EAET and the principal reason for developing the ALT BOR code. The theoretical basis of ALT is given in Section 2.

SECTION 2

PLANE WAVE EXCITATION OF BODIES OF REVOLUTION WITH COMPLEX APERTURES

An $\underset{\sim}{E}$-field formulation, moment method solution of body of revolution (BOR) aperture coupling problems is detailed in Appendix A. Consider a plane containing a straight line and an arbitrarily curved line. The surface of a BOR is traced by the curved line when the plane is rotated with the straight line as its axis. The straight line is called the axis of the BOR and is typically the z axis of a standard $\rho\phi z$ cylindrical coordinate system. The curved line is called the generating curve of the BOR. These and other characteristics of a BOR are discussed in Appendix A, which also contains a description of the equivalent aperture excitation technique (EAET).

The BOR3 computer code [9] implements EAET, but is hampered by an unnecessarily large computer memory requirement; in addition, BOR3 applies only to $\hat{\theta}$-polarized incident waves and does not determine internal $\underset{\sim}{H}$-fields. The ALT BOR code based on the theory in this report extends BOR3 to include ϕ-polarized incident waves and near $\underset{\sim}{H}$-field computation. It also requires about 60 percent less computer memory than does BOR3. In addition, the ALT BOR code employs the aperture loading technique (ALT) suggested in [9(Section 5.2)], but not previously implemented. ALT applies to apertures considerably more complex than simple circumferential openings. The extension of EAET to include ALT is discussed below.

Following the BOR theory of Appendix A, the $\underset{\sim}{E}$-field component tangential to aperture surfaces, $\underset{\sim}{EA}_{tan}$, is expanded as

$$\underset{\sim}{EA}_{tan} = \sum_{np} \left(EA^{t}_{np}\ \hat{t} + EA^{\phi}_{np}\ \hat{\phi}\right) \tag{1}$$

where

$$EA^{t}_{np} = -VA^{t}_{np}\ \delta(t-t_p)\ \frac{e^{jn\phi}}{2\pi} \tag{2}$$

$$EA^{\phi}_{np} = -VA^{\phi}_{np}\ \delta(t-t_p)\ \frac{e^{jn\phi}}{2\pi} \tag{3}$$

The curvilinear coordinate t in (1)-(3) (Figure A-1) traverses the BOR generating curve (latitudinal variation), the ϕ coordinate (Figure A-1) is the azimuthal

(longitudinal) coordinate, $\delta(t)$ is the unit impulse function, the integer $n(-\infty < n < \infty)$ spans the azimuthal BOR (sinusoidal) modes, the interger p (p>0) spans the BOR generating curve triangle functions that reside in an aperture, t_p is the t coordinate of the peak of the p^{th} aperture triangle function, and VA^{t}_{np}, VA^{ϕ}_{np} are coefficients in units of volts.

The surface current, $\underset{\sim}{JA}$, flowing through the apertures when the apertures are excited by (1) is expanded as

$$\underset{\sim}{JA} = \sum_{np} \left(IA^{t}_{np} \, f^{t}_{p}(t) e^{jn\phi} \, \hat{t} + IA^{\phi}_{np} \, f^{\phi}_{p}(t) e^{jn\phi} \, \hat{\phi} \right) \tag{4}$$

where $f^{t}_{p}(t)$ and $f^{\phi}_{p}(t)$ are, respectively, the t-directed and ϕ-directed unit triangle functions divided by the BOR radial coordinate, ρ (ρ is understood to be a function of t), and IA^{t}_{np}, IA^{ϕ}_{np} are coefficients in units of amperes.

Let the p^{th} elements of the matrix column vectors $\vec{IA}^{t}_{n}$, $\vec{IA}^{\phi}_{n}$, $\vec{VA}^{t}_{n}$, and $\vec{VA}^{\phi}_{n}$ be IA^{t}_{np}, IA^{ϕ}_{np}, VA^{t}_{np}, and VA^{ϕ}_{np}, respectively. As discussed in the appendix (Section A-6), the n^{th} mode of aperture surface current coefficients is related to the n^{th} mode of aperture $\underset{\sim}{E}$-field excitation coefficients by the matrix equation

$$\begin{bmatrix} \vec{IA}^{t}_{n} \\ \\ \vec{IA}^{\phi}_{n} \end{bmatrix} = \begin{bmatrix} [YA^{tt}_{n}] & [YA^{t\phi}_{n}] \\ \\ [YA^{\phi t}_{n}] & [YA^{\phi\phi}_{n}] \end{bmatrix} \begin{bmatrix} \vec{VA}^{t}_{n} \\ \\ \vec{VA}^{\phi}_{n} \end{bmatrix} \tag{5}$$

The matrix containing the $[YA^{tt}_{n}]$ etc. submatrices is called the n^{th} mode "aperture admittance matrix." The elements of this matrix are obtained from the BOR moment method theory detailed in Appendix A.

The equivalent aperture excitation technique (EAET) employs (5) in obtaining aperture port voltage source vectors, $\vec{VA}^{t}_{n}$ and $\vec{VA}^{\phi}_{n}$, from "equivalent aperture port current excitation vectors" $\vec{IA}^{t}_{n}$ and $\vec{IA}^{\phi}_{n}$. The $\vec{IA}^{t}_{n}$ and $\vec{IA}^{\phi}_{n}$ are known (Equation (A-122)) from the surface current induced on the BOR after the apertures are covered with perfect conductors. This is discussed in Section A-6. It also is shown in Section A-6 that excitation of the BOR with an equivalent aperture current excitation in terms

of $\vec{IA}_n^t$ and $\vec{IA}_n^\phi$ or, more conveniently, the aperture tangential $\underset{\sim}{E}$-field in terms of $\vec{VA}_n^t$ and $\vec{VA}_n^\phi$ (the apertures are replaced and the external exciting field removed), results in the internal fields of the original problem.

If, however, the aperture has complex edges (e.g., a sleeve-fit seam) or is material filled (e.g., with a dielectric) or both, some current will flow through this aperture "load" when excited by the equivalent current source. This is accounted for with ALT by first identifying the relationship between $\underset{\sim}{EA}_{tan}$ and the surface current, $\underset{\sim}{JL}$, flowing through the load. Corresponding to (4), the expansion for $\underset{\sim}{JL}$ is

$$\underset{\sim}{JL} = \sum_{np} \left(IL_{np}^t \, f_p^t(t) \, e^{jn\phi} \, \hat{t} + IL_{np}^\phi \, f_p^\phi(t) \, e^{jn\phi} \, \hat{\phi} \right) \tag{6}$$

Since the walls of the BOR are thin, $\underset{\sim}{EA}_{tan}$ fills the aperture load surface and is related to $\underset{\sim}{JL}$ through local phenomena relations; e.g., [11]

$$\underset{\sim}{JL} = (\sigma + j\omega(\varepsilon - \varepsilon_0)) \, \underset{\sim}{EA}_{tan} \tag{7}$$

if the aperture is filled with a material of finite conductivity (σ) and permittivity (ε).

Equations (1), (2), (3), and (6) and relationships such as (7) yield

$$\begin{bmatrix} \vec{IL}_n^t \\ \vec{IL}_n^\phi \end{bmatrix} = - \begin{bmatrix} [YL_n^{tt}] & [0] \\ [0] & [YL_n^{\phi\phi}] \end{bmatrix} \begin{bmatrix} \vec{VA}_n^t \\ \vec{VA}_n^\phi \end{bmatrix} \tag{8}$$

where $\vec{IL}_n^t$ and $\vec{IL}_n^\phi$ are matrix column vectors, the p^{th} elements of which are IL_{np}^t and IL_{np}^ϕ, respectively, [0] is the null matrix, and $[YL_n^{tt}]$ and $[YL_n^{\phi\phi}]$ are diagonal matrices. The matrix containing the $[YL_n^{tt}]$ etc. submatrices is called the aperture load matrix.

Continuity of current constrains the total aperture current, $\underset{\sim}{JA}$, to be

$$\underset{\sim}{JA} = -\underset{\sim}{JS} + \underset{\sim}{JL} \tag{9}$$

where -JS is the equivalent aperture excitation current given by (A-120). Equations (4), (A-120), and (6), combined via (9), yield

$$\begin{bmatrix} \vec{IA}_n^t \\ \vec{IA}_n^\phi \end{bmatrix} = - \begin{bmatrix} \vec{IS}_n^t \\ \vec{IS}_n^\phi \end{bmatrix} + \begin{bmatrix} \vec{IL}_n^t \\ \vec{IL}_n^\phi \end{bmatrix} \tag{10}$$

Equation (10), with (5) and (8), yields

$$\left\{ \begin{bmatrix} [YA_n^{tt}] & [YA_n^{t\phi}] \\ [YA_n^{\phi t}] & [YA_n^{\phi\phi}] \end{bmatrix} + \begin{bmatrix} [YL_n^{tt}] & [0] \\ [0] & [YL_n^{\phi\phi}] \end{bmatrix} \right\} \begin{bmatrix} \vec{VA}_n^t \\ \vec{VA}_n^\phi \end{bmatrix} = - \begin{bmatrix} \vec{IS}_n^t \\ \vec{IS}_n^\phi \end{bmatrix} \tag{11}$$

The solution of (11) for $\vec{VA}_n^t$ and $\vec{VA}_n^\phi$ provides $\underset{\sim}{EA}_{tan}$ via (1) through (3). As shown in Appendix A, Section 6, $\underset{\sim}{EA}_{tan}$ can be applied as an excitation resulting in the internal fields of the original problem.

If the q^{th} aperture port is an electrically small, dielectrically-filled sleeve-fit seam (Figure 2), the corresponding elements of (8) lead to

$$IL_{nq}^t = -YL_{nqq}^{tt} \; VA_{nq}^t \tag{12}$$

$$IL_{nq}^\phi = -YL_{nqq}^{\phi\phi} \; VA_{nq}^\phi \tag{13}$$

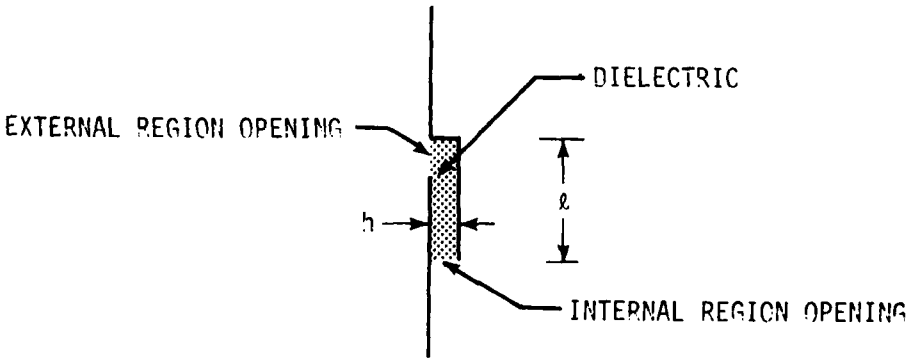

Figure 2. Portion of BOR Generating Curve Containing a Sleeve-Fit Joint

Since the aperture width, h, is much less than λ, VA^{ϕ}_{nq} may be assumed zero. The ϕ-directed "load" current, IL^{ϕ}_{nq}, can easily "skirt" the thin aperture as if the aperture were absent and cancel the equivalent port current excitation, $-IS^{\phi}_{nq}$; thus, by (10), $IA^{\phi}_{nq} = 0$ and (11) is reduced by one equation and one unknown by removing the q^{th} rows of $[YA^{\phi t}_{n}]$, $[YA^{\phi\phi}_{n}]$, and $[YL^{\phi\phi}_{n}]$, and the q^{th} columns of $[YA^{t\phi}_{n}]$, $[YA^{\phi\phi}_{n}]$, and $[YL^{\phi\phi}_{n}]$, and the q^{th} elements of $\vec{VA}^{\phi}_{n}$ and $\vec{IS}^{\phi}_{n}$.

The aperture load admittance, YL^{tt}_{nqq}, for the sleeve-fit seam is approximated as follows. The j_q^{th} triangle function is located with peak at the gap. From (2), the voltage across the gap V_{gap} is approximately

$$V_{gap} = \int_{gap} EA^{t}_{nq}\, dt = - VA^{t}_{nq}\, \frac{e^{jn\phi}}{2\pi} \tag{14}$$

The surface current flowing through the gap, containing both displacement and polarization current, is given, from (6), by

$$I_{gap} = IL^{t}_{nq}\, f^{t}_{q}(t_q)\, e^{jn\phi} \tag{15}$$

or, since $f^{t}_{q}(t_q) = \frac{1}{\rho}$ (note discussion following (4)),

$$I_{gap} = IL^{t}_{nq}\, \frac{e^{jn\phi}}{\rho} \tag{16}$$

The gap susceptance per unit length is

$$\frac{I_{gap}}{V_{gap}} = j\omega C_g \tag{17}$$

where the gap capacitance per unit length C_g is approximately

$$C_g = \frac{\varepsilon \ell}{h} \tag{18}$$

Equations (12), (14), (16), (17), and (18) yield

$$YL^{tt}_{nqq} = \frac{j\omega\epsilon\ell\rho}{2\pi h} \tag{19}$$

In terms of dielectric constant, ϵ_r , free space wave number, k, and free space wave impedance, η,

$$YL^{tt}_{nqq} = \frac{jk\epsilon_r\ell\rho}{2\pi\eta h} \tag{20}$$

SECTION 3

APPLICATION TO A MULTIPLE APERTURE, PARTITIONED CAVITY BOR

The aperture loading technique (ALT) was applied to a BOR defined by the generating curve of Figure 3. The excitation was the nose-on x polarized unit plane wave

$$\underset{\sim}{E}^e = -e^{-jkz}\,\hat{x}\ \text{V/m} \tag{21}$$

defined with reference to the coordinate system shown in Figures A-1 and A-2 and where k is the wave number corresponding to 300MHz. The body had two apertures: open front end and a sleeve-fit, dielectric-filled seam. A conducting partition was located at z = 0.255m.

The partition was assumed to meet the outer wall at z = 0.255m since h was electrically very small. This formed a three-surface junction which could not be modeled with the ALT BOR code without significant code modification. Variations to the Figure 3 BOR multiple surface junctions are shown in Figures 4 and 5. An accurate solution to the Figure 3 aperture coupling problem was achieved by properly defining the Figures 4 and 5 problems and combining their solutions within the equivalent aperture excitation technique (EAET) framework described below.

The EAET naturally divides into three parts. Part 1 uses BOR scattering theory (Sections A-1 through A-3) to obtain the external scattering current with the apertures removed (shorted). Here the Figure 4 BOR (solid line) applies exactly. Part 2 uses BOR theory (Section A-6) to obtain an aperture voltage excitation by computing an aperture admittance matrix and combining it with an equivalent aperture current excitation. The current excitation is the negative of the external scattering current induced on the aperture shorts in Part 1. (The ALT improves this aperture voltage excitation computation by adding an aperture load admittance to the aperture admittance matrix as described in Section 2.) The aperture voltage excitation is obtained by exciting <u>both external and internal regions simultaneously</u>. Neither Figures 4 nor 5 model the Figure 3 body exactly for this computation. Since the body is electrically thin at 300 MHz, the internal fields decay rapidly away from the aperture and the Figure 4 model is expected to be adequate for computing the aperture voltage excitation.

Part 3 of the EAET uses BOR theory (Sections A-4 and A-5) to compute the internal fields by applying the aperture voltage excitation to the BOR. This computation

COORDINATES ($\times 10^{-2}$ m)

POINT	ρ	z
1	0	0
2	3.69	0
3	6.40	19.40
4	6.40	20.94
5	6.40	23.525
6	6.40	25.5
7	6.40	110.0
8	0	110.0
9	0	25.5

$\ell = 2.625 \times 10^{-2}$ m

$h = 0.25 \times 10^{-2}$ m

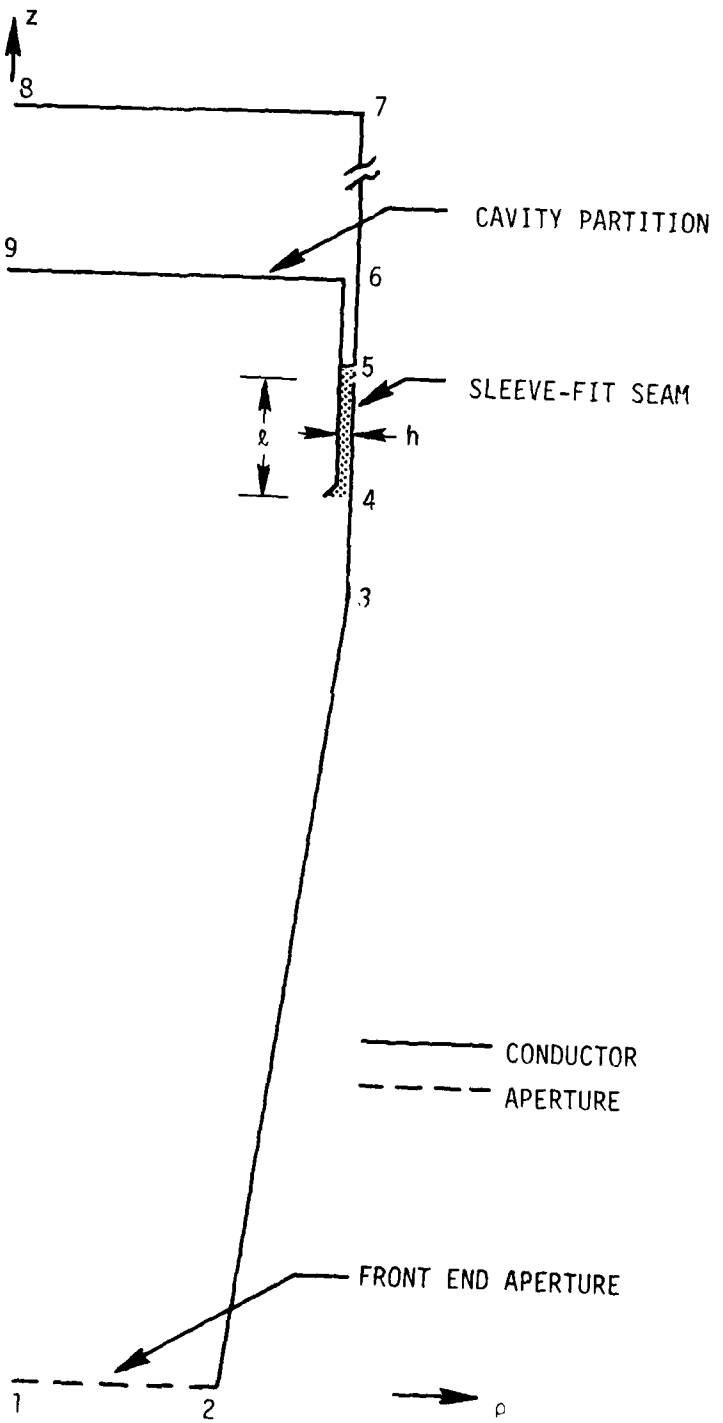

Figure 3. Generating Curve of a Conducting BOR with an Open Front End, a Partitioned Cavity, and a Dielectric Filled, Sleeve-Fit Seam

COORDINATES ($\times 10^{-2}$ m)

POINT	ρ	z
1a	0	-3.15
2	3.69	0
3	6.40	19.40
5	6.40	23.525
6a	6.40	106.35
7	6.40	110.0
8	0	110.0
8a	0	112.75

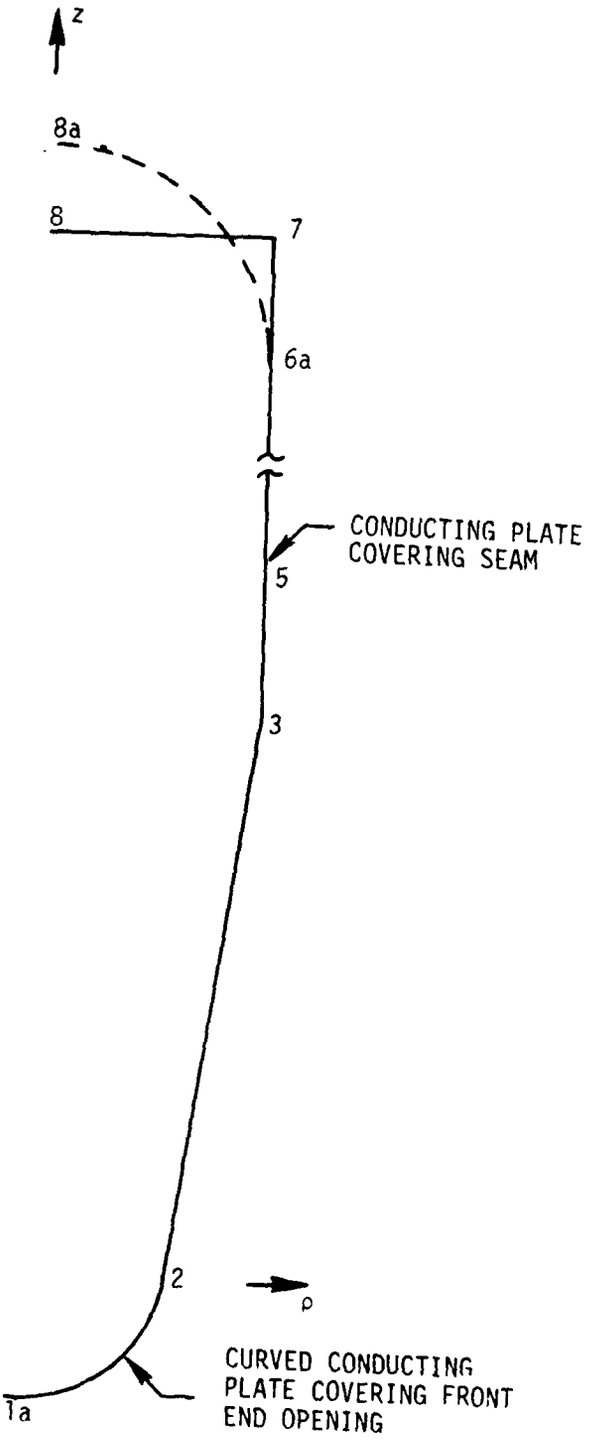

Figure 4. Generating Curve for Determining Aperture Voltage Excitation Due to Plane Wave Externally Incident on Figure 3 Body.

COORDINATES ($\times 10^{-2}$ m)

POINT	ρ	z
1a	0	-3.15
2	3.69	0
3	6.40	19.4
4	6.40	20.9
6	6.40	25.5
9	0	25.5

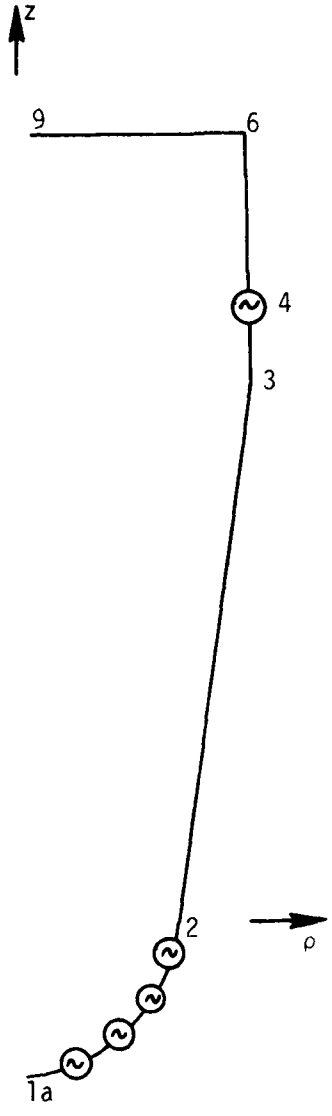

Figure 5. Generating Curve for Determining Internal Fields of Figure 3 Problem from Aperture Voltage Excitation

results in the same internal fields when applied to the Figure 5 body as for the Figure 3 body.

This scheme of using the Figure 4 body for Parts 1 and 2 of the EAET and the Figure 5 body for Part 3 was expected to result in a good approximation to the internal field of the Figure 3 body when excited by (21).

The numbers of triangle functions on the Figures 4 and 5 generating curves were chosen to provide the desired resolution in near field. This was critical only for the Figure 5 geometry since, as discussed above, the Figure 4 geometry was not used for near-field computation. The Figure 4 expansion functions must be sufficient to resolve surface current and aperture voltage.

Only the n = 1 BOR mode fields and currents are excited by axially incident plane waves. The incident field $\underset{\sim}{E}^e$ given by (21) is θ directed in the $\phi = 0$ plane. From (A-55), therefore, the induced surface current has the form

$$\left.\begin{array}{l}\text{surface current due}\\ \text{to } \underset{\sim}{E}^e \text{ of (21)}\end{array}\right\} = J^t \cos\phi\,\hat{t} + J^\phi \sin\phi\,\hat{\phi} \qquad (22)$$

where t is the generating curve coordinate (Figure A-1). Surface currents computed by the ALT BOR code are prone to exhibit severe oscillation particularly if the BOR surface has edges and the BOR is thin. This was experienced by Davis and Mittra [15]. The problem was analyzed by Glisson and Wilton [16], and they developed a corrected BOR moment method code. Another corrected BOR moment method code recently was developed by Mautz and Harrington [13]. The Mautz and Harrington version, more closely resembling the BOR code upon which the ALT BOR code has been developed, is in the process of being adapted to the ALT BOR code.

The present version of ALT BOR code, meanwhile, has been applied to the Figure 3 problem via the Figures 4 and 5 geometries as described above. The computed scattering current on the Figure 4 geometry exhibited severe oscillations in both J^t and J^ϕ. In attempting to reduce this oscillation, the tail section of the Figure 4 geometry was rounded as indicated by the dashed line in Figure 4. This avoided the edge at reference point 7. The curved path was chosen such that the path lengths 6a to 8a and 6a to 7 to 8 were equal. The generating curve then was segmented (for triangle expansion functions) in a manner maintaining less than 2:1 variation in adjacent segment sizes. The rounded tail section and small variation in adjacent segment sizes resulted in the J^t and J^ϕ curves of Figure 6. The generating curve was divided into

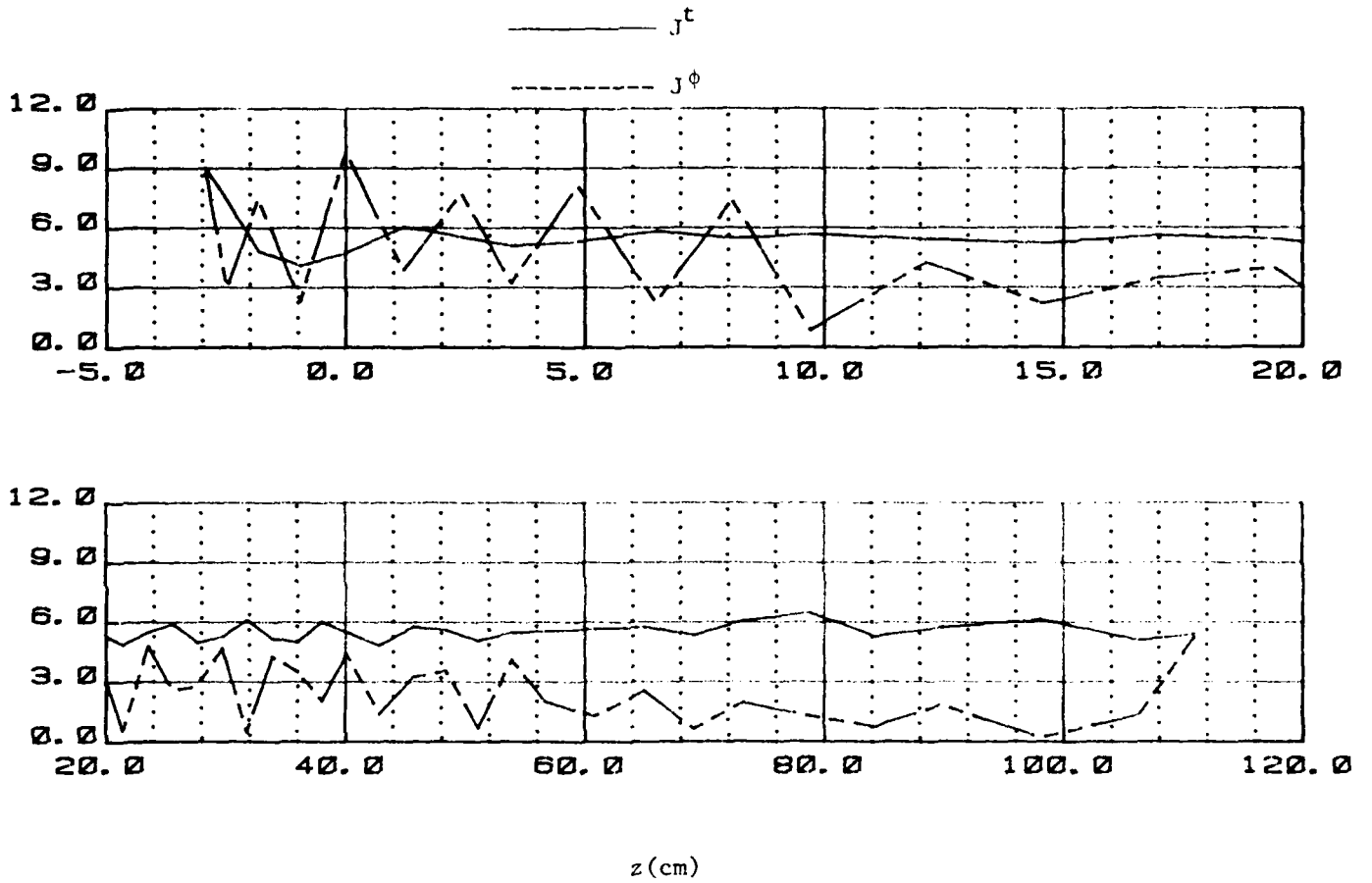

Figure 6. Induced Surface Current on Figure 4 Body versus z (axial coordinate). Incident Wave Given by (21). Frequency = 300 MHz. (Continued on next page.)

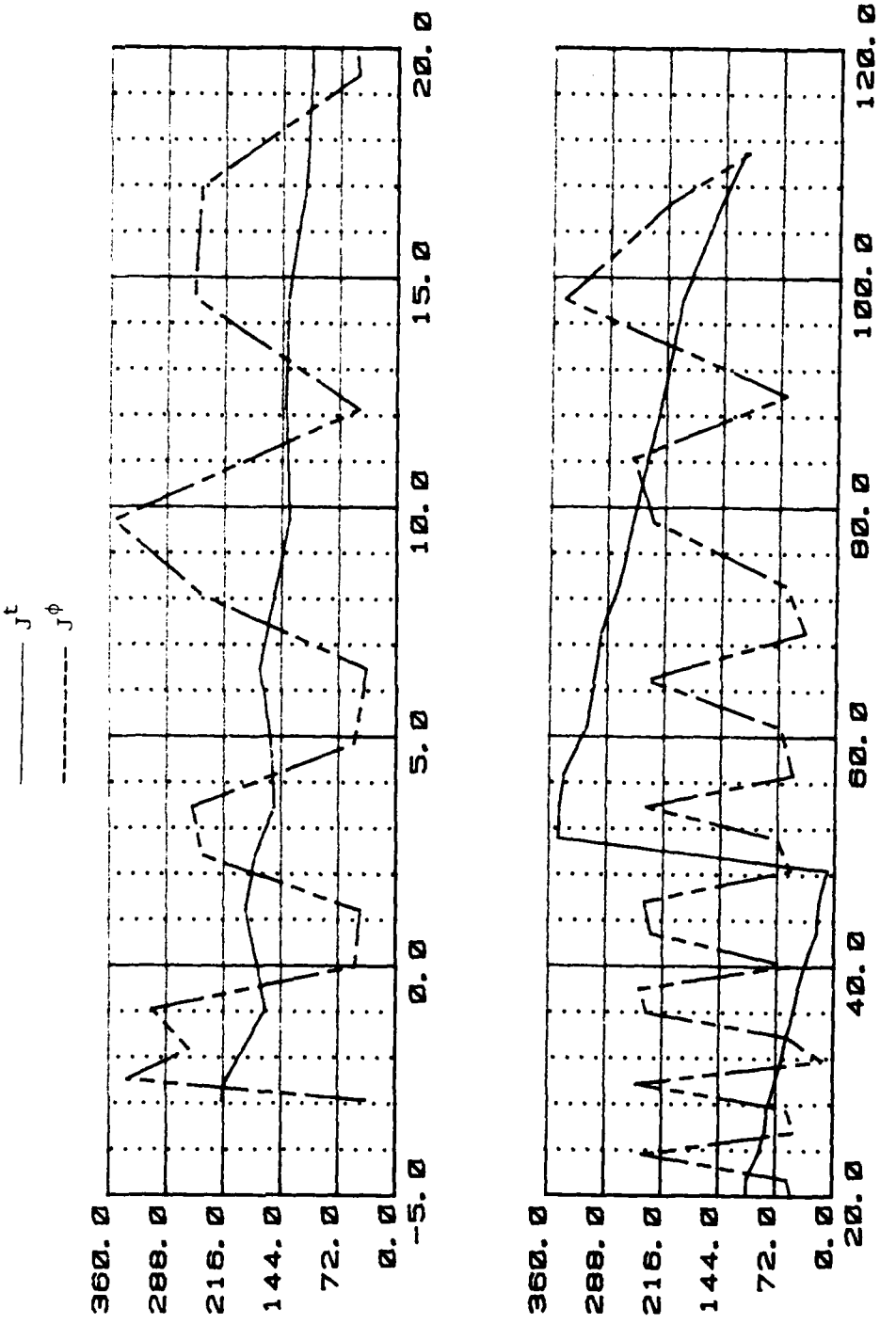

Figure 6. Continued

86 segments (42 triangle functions). The J^t current then was reasonably smooth. The J^z current, however, still oscillated severely. Nevertheless, the ALT/EAET was continued in the belief that the internal fields were not strongly affected by the oscillation in J^z. In Figure 5, the currents are plotted vs. the z coordinate of the generating curve. Each plot point corresponds to the peak of a triangle function.

Two sets of five aperture voltages sources (four at the front end and one at the sleeve fit seam) were determined. One set corresponded to the air filled seam and one to the dielectric filled seam (dielectric constant $\varepsilon_r = 5.5$). These sources were applied to the Figure 5 generating curve as indicated in Figure 5, and the internal E- and H-fields computed. The Figure 5 generating curve was divided into 82 segments (40 triangle functions).

The internal fields have the form (note (A-78) and (A-118))

$$\left.\begin{array}{l}\text{E-field due to} \\ \underset{\sim}{E}^e \text{ of (21)}\end{array}\right\} = E_\rho \cos\phi\,\hat{\rho} + E_z \cos\phi\,\hat{z} + E_\phi \sin\phi\,\hat{\phi} \qquad (23)$$

$$\left.\begin{array}{l}\text{H-field due to} \\ \underset{\sim}{E}^e \text{ of (21)}\end{array}\right\} = H_\rho \sin\phi\,\hat{\rho} + H_z \sin\phi\,\hat{z} + H_\phi \cos\phi\,\hat{\phi} \qquad (24)$$

Contour maps of the magnitude of E_ρ, E_z, E_ϕ, ηH_ρ, ηH_z, and ηH_ϕ in dB are shown in Figures 7 and 8 where η is the free space wave impedance. The resolution of computed internal field data to achieve these plots was 0.005 m within 0.02 m of an aperture and 0.01 m elsewhere. The field contours were smoothed wherever oscillations were likely caused by the granularity of the surface current representation. Field oscillations were evident primarily within a centimeter or so of a conducting surface.

The fields (Figure 8) in the dielectric filled seam case were approximately 25 dB below those (Figure 9) for the air filled seam case near the seam. This could have been predicted by comparing the n = 1 mode radiation admittance ($YA^{tt}_{1,5,5}$ of (11))* at the seam with the aperture load admittances ($YL^{tt}_{1,5,5}$ of (20)) for the air filled seam and the dielectric filled seam as follows. The aperture voltage sources were determined from the equivalent aperture current sources (the latter are independent of aperture loading) by adding together the radiation and load admittances and inverting the sum as suggested by (11). In the problem under consideration

* The 5,5 matrix element corresponds to the seam aperture for this problem.

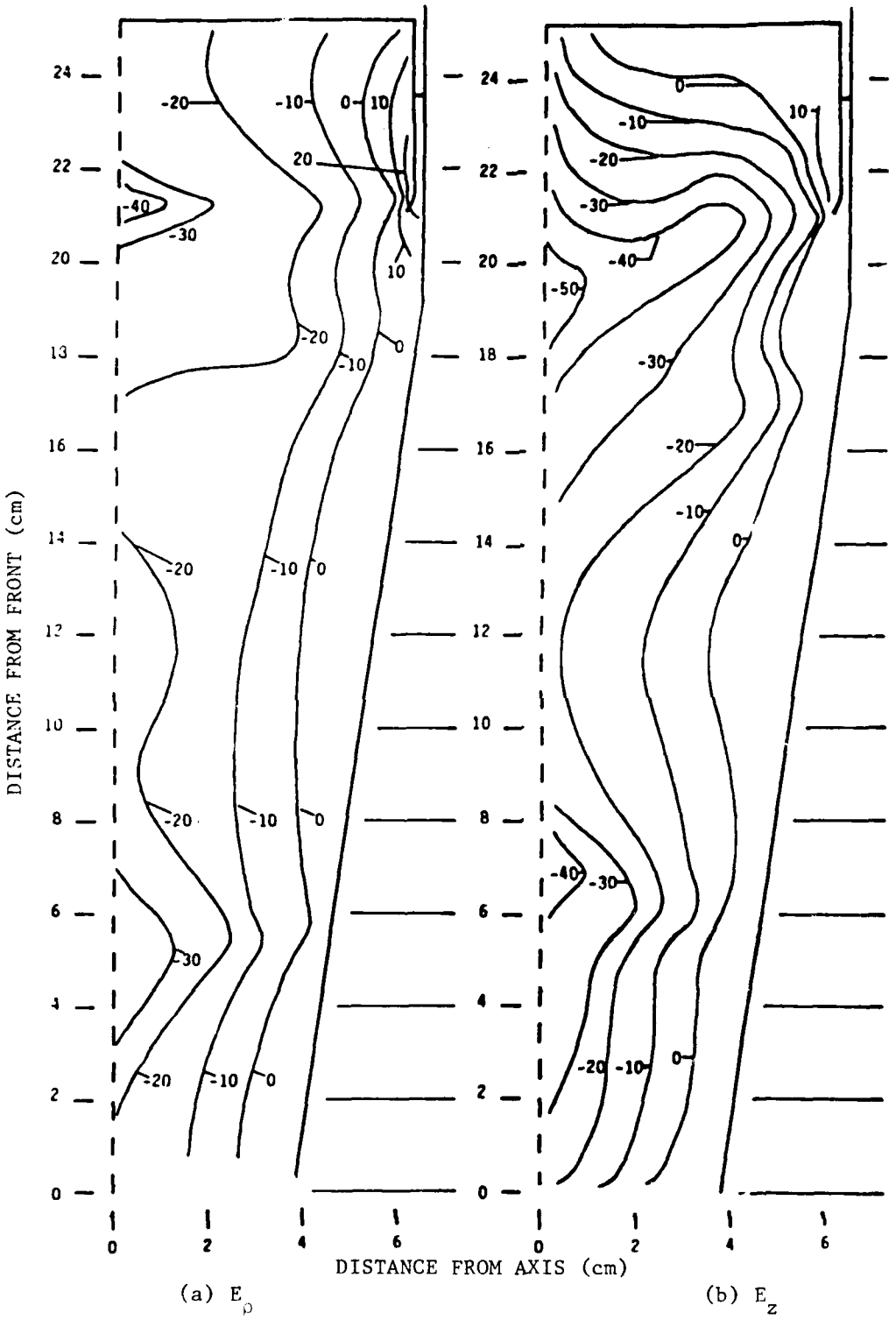

Figure 7. Field Contours in dB (Air-Filled Sleeve Fit Seam): E_ρ, E_z, ηH_ϕ in $\phi = 0$ Plane; E_ϕ, ηH_ρ, ηH_z in $\phi = \pi/2$ Plane; Incident E-Field = Incident Wave Given by (21).

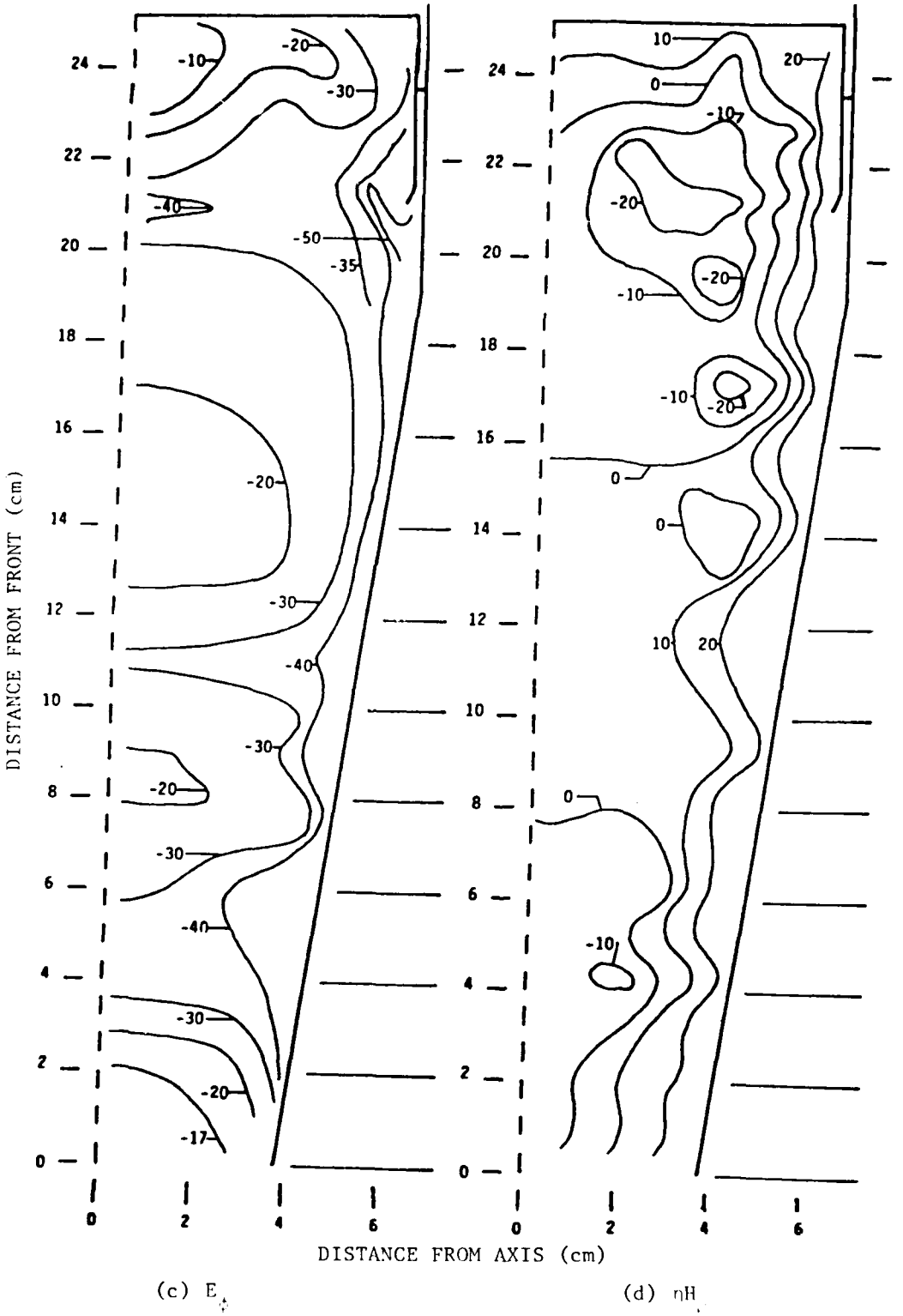

Figure 7. Continued

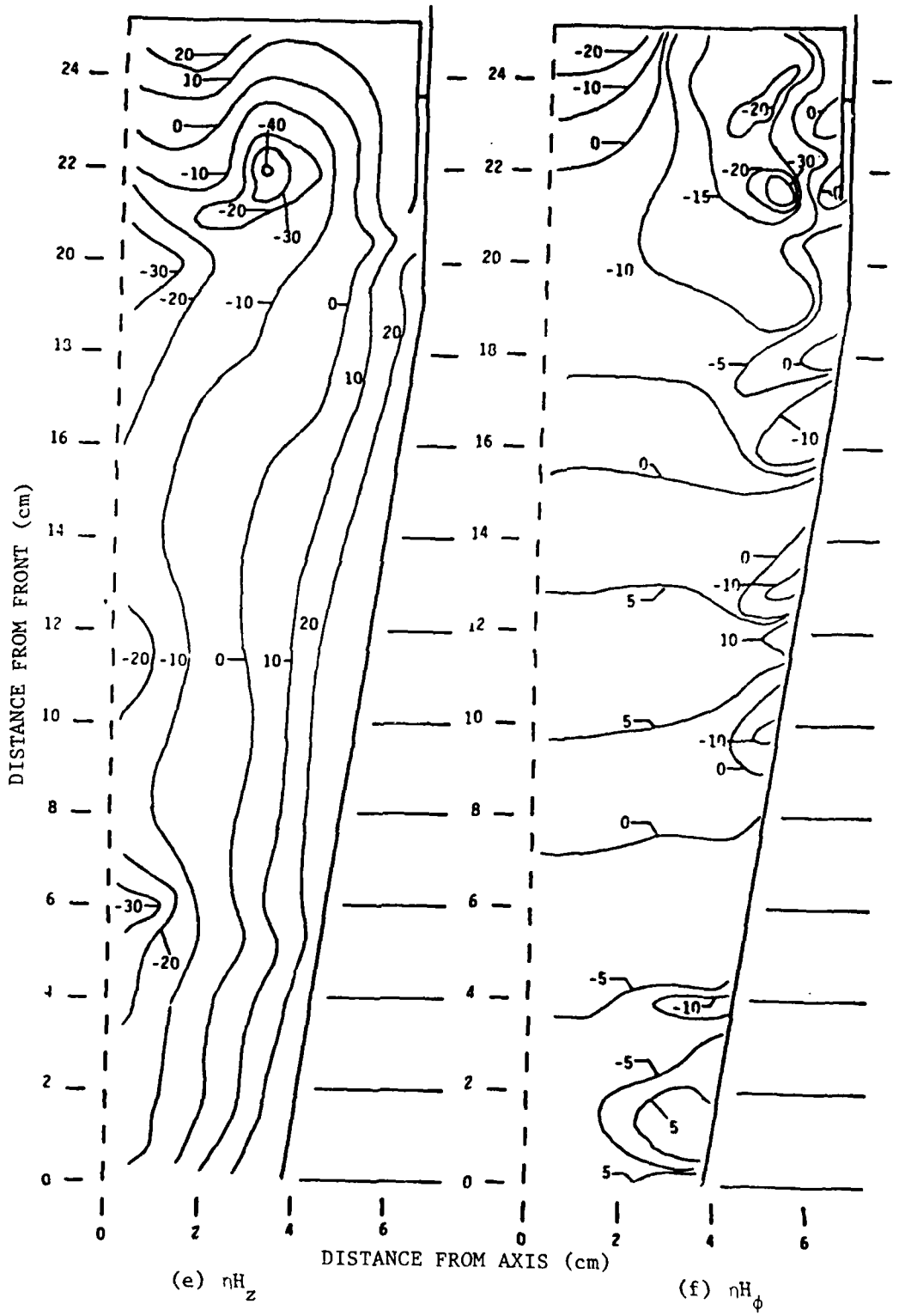

Figure 7. Continued

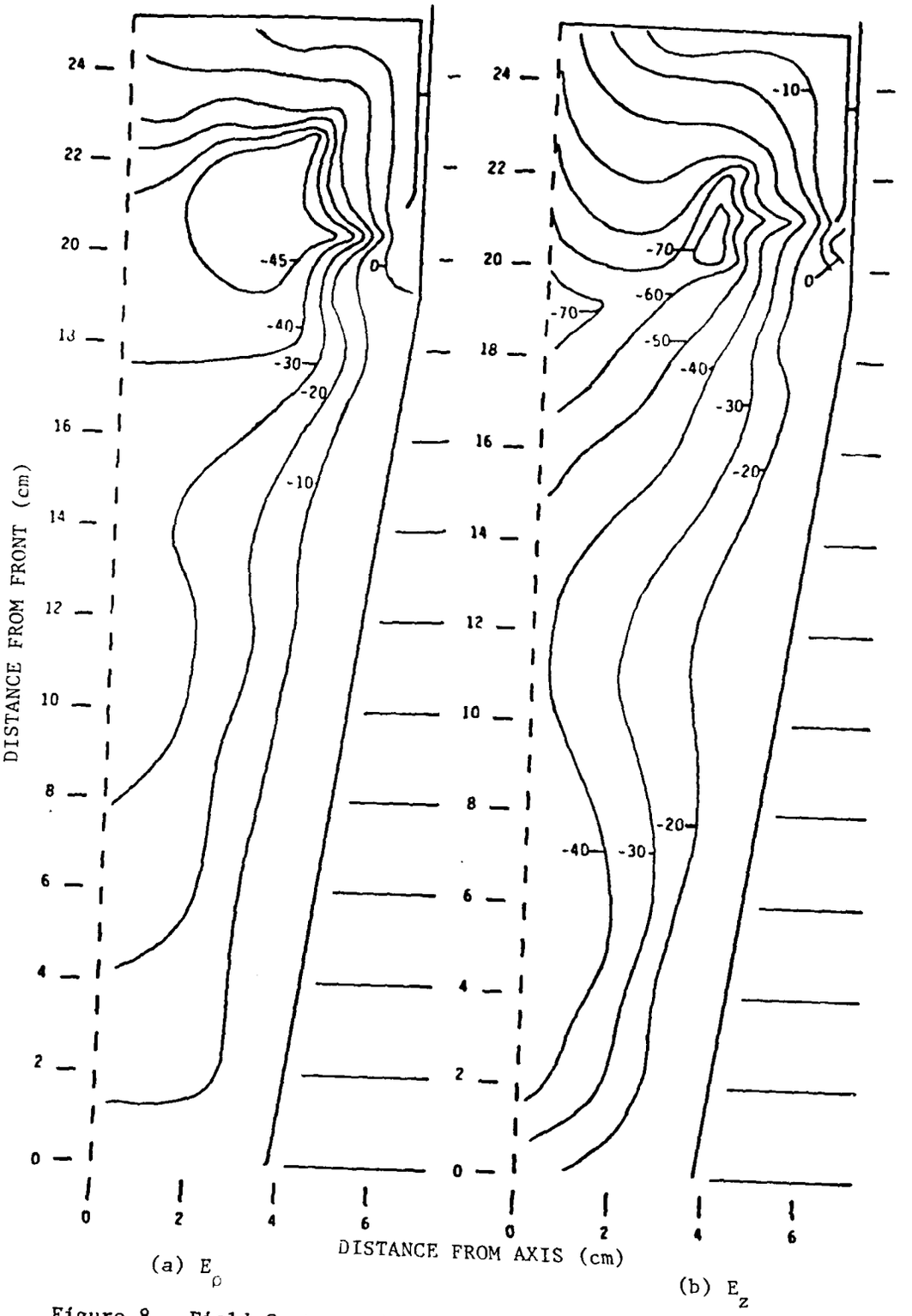

Figure 8. Field Contours in dB (Dielectric-Filled Sleeve Fit Seam): E_ρ, E_z, ηH_ϕ in $\phi = 0$ Plane; E_ϕ, ηH_ρ, ηH_z in $\phi = \pi/2$ Plane; Incident E-Field = Incident Wave Given by (21).

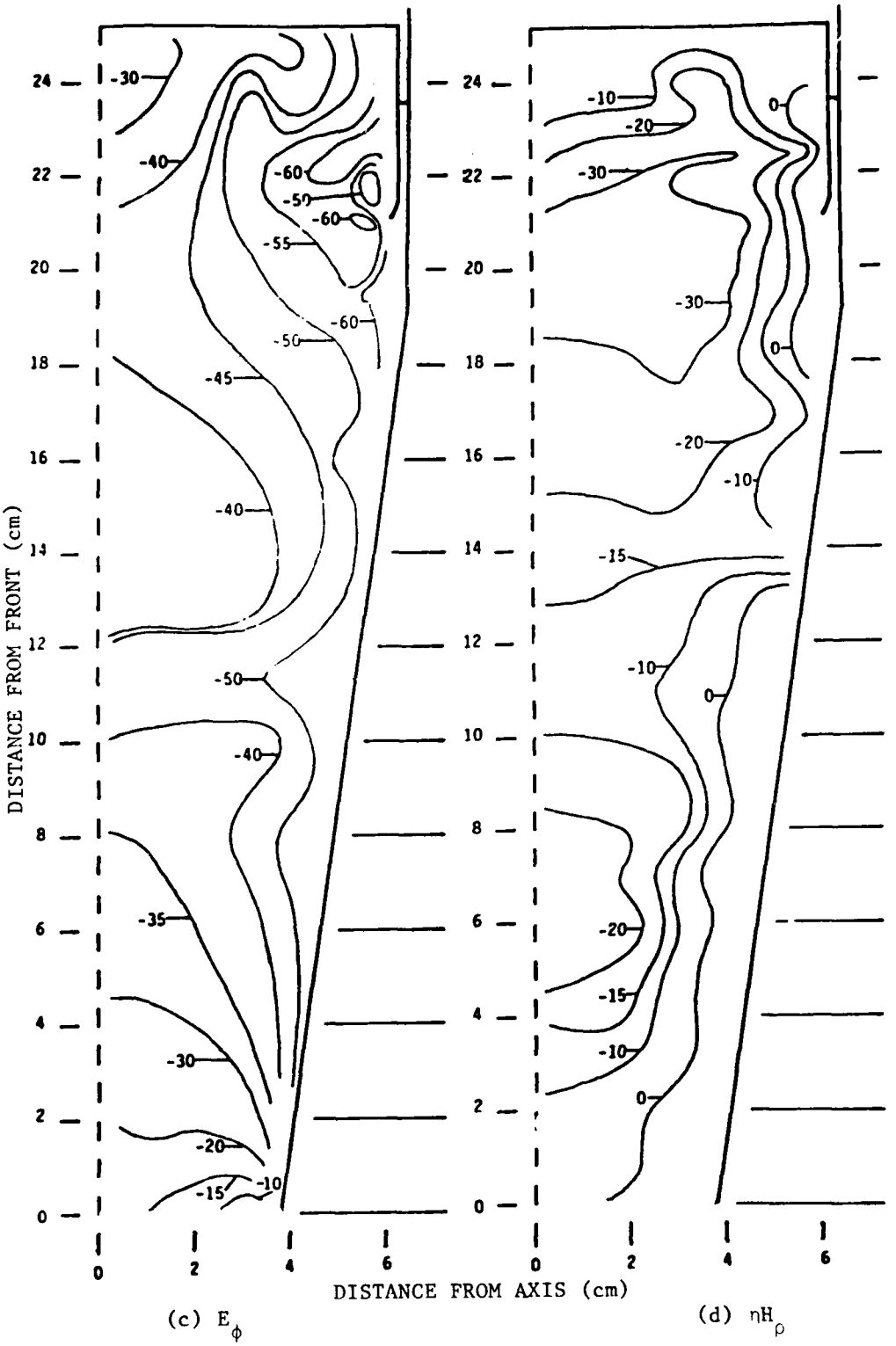

Figure 8. Continued

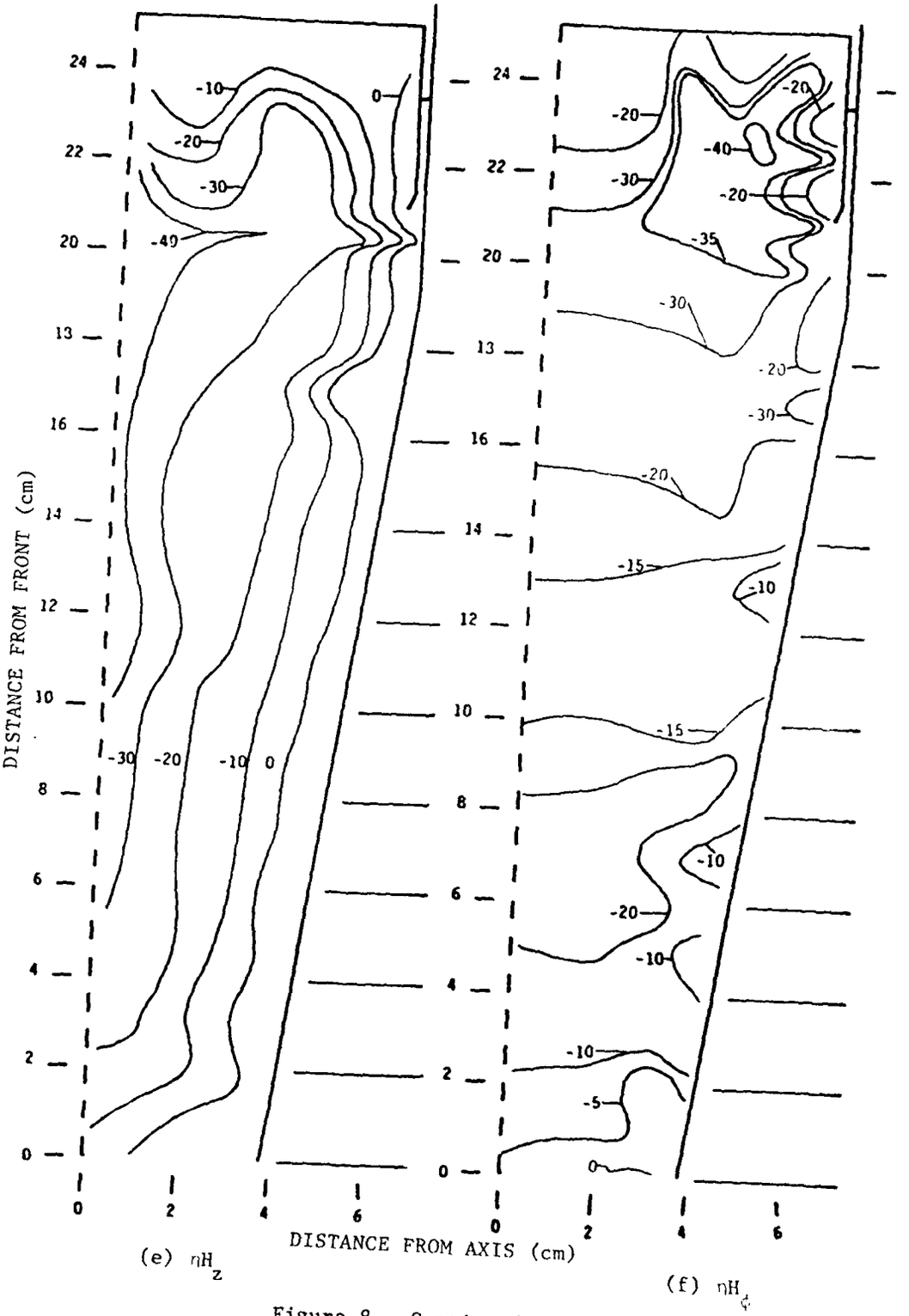

Figure 8. Continued

$$YA^{tt}_{1,5,5} = 0.04 - j1.34 \text{ mS}$$

and for the air filled seam and dielectric filled seam respectively

$$YL^{tt}_{1,5,5}\Big|_{\epsilon_r = 1.0} = j1.78 \text{ mS}$$

$$YL^{tt}_{1,5,5}\Big|_{\epsilon_r = 5.5} = j9.82 \text{ mS}$$

Thus, the total admittance in each case was

$$Y_{air} = YA^{tt}_{1,5,5} + YL^{tt}_{1,5,5}\Big|_{\epsilon_r = 1.0} = 0.04 + j0.44 \text{ mS}$$

$$Y_{diel} = YA^{tt}_{1,5,5} + YL^{tt}_{1,5,5}\Big|_{\epsilon_r = 5.5} = 0.04 + j8.48 \text{ mS}$$

The smaller Y_{air} resulted in a correspondingly larger aperture voltage excitation. The air filled seam nearly "resonated" the aperture by almost cancelling the radiation inductive reactance. The dielectric filled seam, on the other hand, introduced a shorting effect by adding a large aperture capacitance to the relatively small aperture radiation reactance. Since

$$20 \log |Y_{air}/Y_{diel}| \simeq -25.6 \text{ dB}$$

the $\simeq$25 dB smaller fields for the dielectric filled seam than for the air filled seam was to be expected.

The air filled seam problem has been analyzed previously by a time stepping solution to the time dependent differential Maxwell equations [17]. Maxwell's equations were solved at each of many time steps until a steady state solution resulted. Their results differ significantly from ours. Some of this difference, perhaps, can be attributed to the unwarrented oscillations in surface current as computed with the present ALT BOR code. The ALT BOR code is presently undergoing significant improvement in this area as mentioned above.

The ALT BOR code was implemented on a DEC PDP-11/34 minicomputer. The above problem required hours of central processing time with this machine due to the enormous amount of input/output time necessary to accomodate large complex matrices (orders approximating 80) with 128K bytes of main memory.

The equivalent approximate run time assuming the entire problem was solved with main memory (no peripheral storage) is given by

$$\text{Time} = n(A(m_1^3 + m_2^3 + a^3) + B(m_1^2 + m_2^2 + a^2) + Ci(m_1^3 + m_2^3 + a^3) + Dim_1 + Epm_2) \tag{25}$$

where

m_1 = number of triangle functions on the exterior problem generating curve (e.g., that of Figure 4)

m_2 = number of triangle functions on the interior problem generating curve (e.g., that of Figure 5)

a = number of triangle functions within the apertures

p = number of near field points

i = number of different incident plane wave directions

n = number of BOR modes

A, B, C, D, and E are system dependent constants.

A second computation with a change in aperture loading (e.g., adding dielectric material to the sleeve-fit seam of Figure 3) requires only the additional time corresponding to doubling Aa^3, $Ci(m_2^2 + a^2)$, and Epm_2.

The coefficients in (25) for a Honeywell 6000 series system are

$A = 3.2 \times 10^{-3}$

$B = 1.3 \times 10^{-2}$

$C = 5.0 \times 10^{-5}$

$D = 3.2 \times 10^{-2}$

$E = 0.87$

where the near field computation time coefficient E is for total E-field (scattered plus impressed).

The principal computer main memory constraint is $m_1^2 + m_2^2$ complex words, or if only the "exterior or "interior" problem matrix is in main memory at one time, the larger of m_1^2 and m_2^2.

SECTION 4

REFERENCES

1. J. R. Mautz and R. F. Harrington, H-Field, E-Field and Combined Field Solutions for Bodies of Revolution, ECE Dept., Syracuse University, TR-77-2, February 1977. (See also computer program description TR-77-3, May 1977.)

2. E. A. Wolff, Antenna Analysis, John Wiley and Sons, Inc., New York 1966, pg. 61.

3. V. I. Krylov, Approximate Calculation of Integrals, translated by A. H. Stroud, Macmillian, Co., New York, 1962, Appendix A.

4. D. Capozzolo and H. K. Schuman, Computer Code User Manual for Equivalent Aperture Excitation Technique Applied to Coupling Through Material Filled Odd Shaped Apertures in Bodies of Revolution, Atlantic Research Corporation under Contract to Rome Air Development Center, RBC, Rome, New York, 1980.

5. M. Abramowitz and I. A. Stegun, Handbook of Mathematical Functions, U. S. Govt. Printing Office, Washington, D. C. (Natl. Bur. Std. U. S. Appl. Math. Ser. 55), 1964, pg. 360.

6. R. M. Bevensee, S3F - SYR/LLL1 The Syracuse Computer Code for Radiation and Scattering from Bodies of Revolution, Extended for Near-Field Computations, Report No. UCRL-51622, prepared for U. S. Atomic Energy Commission under Contract No. W-7405-Eng-48 with the Lawrence Livermore Laboratory, University of California, Livermore, CA, May 1974.

7. R. F. Harrington, Time-Harmonic Electromagnetic Fields, McGraw Hill Book Co., 1961.

8. S. A. Schelkunoff, "Field Equivalence Theorems," Comm. on Pure and Applied Math., Vol. 4, pp. 43-59, June 1951.

9. H. K. Schuman and D. E. Warren, Coupling Through Rotationally Symmetric Apertures in Cavities of Revolution, RADC-TR-77-214, Rome Air Development Center, Griffiss AFB, Rome, NY 13441, June 1977. See also, IEEE Trans. Ant. Propg., Vol. AP-26, No. 6, pp. 778-783, November 1978. AD# A042 093.

10. A. W. Glisson and D. R. Wilton, "A simple Approach to the Problem of Coupling Through Azimuthally Symmetric Apertures in Bodies of Revolution," 1978 IEEE Antennas and Propagation International Symposium, Washington, D. C., pp. 215-218, May 1978.

11. R. F. Harrington and J. R. Mautz, "An Impedance Sheet Approximation for Thin Dielectric Shells," IEEE Trans. Ants. Propg., Vol. AP-23, pp. 532-534, July 1975.

12. R. F. Harrington and J. R. Mautz, Radiation and Scattering from Bodies of Revolution, Report AFCRL-69-0305, Air Force Cambridge Research Laboratories, (under contract with Syracuse University), July 1969.

13. J. R. Mautz and R. F. Harrington, "An Improved E-Field Solution for a Conducting Body of Revolution," RADC-TR-80-194, Air Force Systems Command, Griffiss AFB, NY 13441, June 1980.

14. L. N. Medgyesi-Mitschang, Aperture-Coupled Fields in Asymmetric Bodies, McDonnell Douglas Research Laboratories Report 80-5, 1980.

15. W. A. Davis and R. Mittra, "A New Approach to the Thin Scatterer Problem Using Hybrid Equations," IEEE Trans. Ants. Propg., Vol. AP-25, pp. 402-406, May 1977.

16. A. W. Glisson and D. R. Wilton, "Simple and Efficient Numerical Techniques for Treating Bodies of Revolution," RADC-TR-79-22, Air Force Systems Command, Griffiss AFB, NY 13441, March 1979. AD# A067 361.

17. A. Taflove, "Time Domain Solutions for Electromagnetic Problems," RADC-TR-78-142, Air Force Systems Command, Griffiss AFB, NY 13441, June 1978. AD# A056 728.

APPENDIX A

BODY OF REVOLUTION SCATTERING AND APERTURE COUPLING

This appendix contains the description of an extension to the Mautz/ Harrington [1] moment method solution of an $\underset{\sim}{E}$-field formulation for scattering from closed conducting bodies of revolution (BORs). The following conditions are applicable:

1. The BOR may have edges (disks, tubular cylinders, etc.),
2. The BOR may have apertures that are rotationally symmetric about the BOR axis,
3. An electrically thin aperture may be of complex shape (e.g., "sleeve" fit) or material filled,
4. The scattered near electric fields, internal and external to the BOR, can be computed, and
5. The scattered near magnetic fields, internal and external to the BOR, can be computed.

The development follows closely that of Mautz and Harrington.

It is desired to determine the electric surface current and the near scattered field of a perfectly conducting BOR (Figure A-1) excited by an incident plane wave. In Figure A-1, ρ, ϕ, and z are cylindrical coordinates and t and ϕ form an orthogonal curvilinear coordinate system on the surface, S, of the BOR. The t coordinate tranverses the "generating curve" of the BOR. $\hat{t}$ and $\hat{\phi}$ are orthogonal unit vectors in the t and ϕ directions, respectively. The coordinate origin is on the axis of the BOR but not necessarily at the lower pole as in Figure A-1. Figure A-2 defines the propagation vector, $\underset{\sim}{k}_e$, of the incident plane wave and the transmitter coordinate θ_e. Note that the transmitter ϕ coordinate is zero so that $\underset{\sim}{k}_e$ lies parallel to the xz plane. In Figure 2, $\hat{\theta}_e$ and $\hat{\phi}_e$ are unit vectors in the θ_e and y directions, respectively.

Consider separately a θ polarized incident plane wave defined by

$$\underset{\sim}{E}^e = \hat{\theta}_e \, e^{-j\underset{\sim}{k}_e \cdot \underset{\sim}{r}} \tag{A-1}$$

and a ϕ polarized incident plane wave defined by

$$\underset{\sim}{E}^e = \hat{\phi}_e \, e^{-j\underset{\sim}{k}_e \cdot \underset{\sim}{r}} \tag{A-2}$$

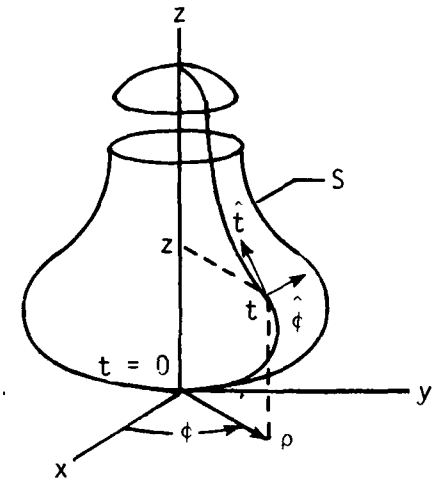

Figure A-1. Body of Revolution and Coordinate System

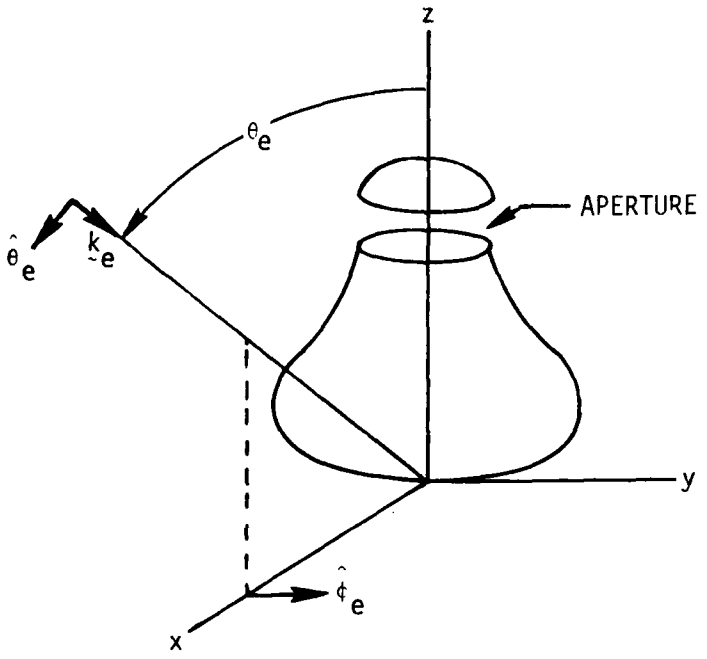

Figure A-2. Plane Wave Scattering by a Conducting Body of Revolution

where $\underset{\sim}{E}^e$ denotes the incident electric field and $\underset{\sim}{r}$ is the radius vector from the origin. Either plane wave gives rise to t and ϕ directed electric surface currents on S.

1. $\underset{\sim}{E}$-FIELD SOLUTION

The $\underset{\sim}{E}$-field solution is obtained by applying the method of moments to the $\underset{\sim}{E}$-field integral equation. The $\underset{\sim}{E}$-field integral equation is derived by setting the component tangential to S of the total electric field equal to zero on S.

The boundary condition that the total tangential electric field is zero on S is written as

$$-\underset{\sim}{E}^s_{tan} = \underset{\sim}{E}^e_{tan} \qquad \text{on S} \tag{A-3}$$

where $\underset{\sim}{E}^s$ is the electric field due to the electric surface current on S and $\underset{\sim}{E}^e$ is the incident electric field given by either (A-1) or (A-2). The subscript tan denotes tangential components on S.

The field $\underset{\sim}{E}^s$ can be expressed in terms of a vector potential, $\underset{\sim}{A}$, and a scalar potential, Φ, as

$$\underset{\sim}{E}^s = -j\omega\underset{\sim}{A}(\underset{\sim}{J}) - \underset{\sim}{\nabla}\Phi(\underset{\sim}{J}) \tag{A-4}$$

where

$$\underset{\sim}{A}(\underset{\sim}{J}) = \mu \iint_S \underset{\sim}{J}(\underset{\sim}{r}') \frac{e^{-jk|\underset{\sim}{r}-\underset{\sim}{r}'|}}{4\pi|\underset{\sim}{r}-\underset{\sim}{r}'|} ds' \tag{A-5}$$

$$\Phi(\underset{\sim}{J}) = \frac{1}{\varepsilon} \iint_S \sigma \frac{e^{-jk|\underset{\sim}{r}-\underset{\sim}{r}'|}}{4\pi|\underset{\sim}{r}-\underset{\sim}{r}'|} ds' \tag{A-6}$$

Here, $\underset{\sim}{r}$ and $\underset{\sim}{r}'$ are vectors to the field and source points, respectively, $\underset{\sim}{J}(\underset{\sim}{r}')$ is the electric surface current on S, k is the propagation constant, μ is the permeability, ε is the permittivity, and σ is the surface charge given by

$$\sigma = -\frac{1}{j\omega} \lim_{\Delta S \to 0} \left(\frac{\oint_C \underset{\sim}{J}(\underset{\sim}{r})\cdot\hat{n}dc}{\Delta S} \right) = -\frac{1}{j\omega} \underset{\sim}{\nabla}_s \cdot \underset{\sim}{J}(\underset{\sim}{r}) \tag{A-7}$$

where $\hat{n}$ is the unit vector tangential to S and normal to the curve, C, which bounds the small portion, ΔS, of S. $\hat{n}$ points away from ΔS. The operator $\nabla_s \cdot$ is the surface divergence on S.

Following the method of moments, J is expanded as

$$\underset{\sim}{J} = \sum_{n,j} \left(I^t_{nj} \underset{\sim}{J}^t_{nj} + I^\phi_{nj} \underset{\sim}{J}^\phi_{nj} \right) \tag{A-8}$$

where I^t_{nj} and I^ϕ_{nj} are coefficients to be determined and $\underset{\sim}{J}^t_{nj}$ and $\underset{\sim}{J}^\phi_{nj}$ are expansion functions defined by

$$\underset{\sim}{J}^t_{nj} = \hat{t} f^t_j(t)\, e^{jn\phi}$$

$$\underset{\sim}{J}^\phi_{nj} = \hat{\phi} f^\phi_j(t)\, e^{jn\phi} \tag{A-9}$$

The choice of functions $f^t_j(t)$ and $f^\phi_j(t)$ is discussed below. The integral over S of the dot product of (A-3) with each one of a collection of testing functions, $\underset{\sim}{W}^t_{mi}$, $\underset{\sim}{W}^\phi_{mi}$, defined by

$$\underset{\sim}{W}^t_{mi} = \hat{t} f^t_i(t)\, e^{-jm\phi}$$

$$\underset{\sim}{W}_{mi} = \hat{\phi} f^\phi_i(t)\, e^{-jm\phi} \tag{A-10}$$

is taken to obtain the matrix equation

$$\sum_n \left(\left[Z^{tt}_{mn} \right] \vec{I}^t_n + \left[Z^{t\phi}_{mn} \right] \vec{I}^\phi_n \right) = \vec{V}^t_m$$

$$\sum_n \left(\left[Z^{\phi t}_{mn} \right] \vec{I}^t_n + \left[Z^{\phi\phi}_{mn} \right] \vec{I}^\phi_n \right) = \vec{V}^\phi_m \tag{A-11}$$

where the [Z]s are square matrices whose ij^{th} elements are defined by

$$Z^{pq}_{mnij} = \iint_S \underset{\sim}{W}^p_{mi} \cdot \left(j\omega \underset{\sim}{A}(\underset{\sim}{J}^q_{nj}) + \nabla\phi(\underset{\sim}{J}^q_{nj}) \right) ds \tag{A-12}$$

where p may be either t or ϕ and q may be either t or ϕ. Also, $\vec{V}_m^t$ and $\vec{V}_m^\phi$ are column vectors whose i^{th} elements are given by

$$V_{mi}^p = \iint_S \underset{\sim}{W}_{mi}^p \cdot \underset{\sim}{E}^e ds \tag{A-13}$$

where p may be either t or ϕ. Lastly, $\vec{I}_n^t$ and $\vec{I}_n^\phi$ are column vectors of the coefficients I_{nj}^t and I_{nj}^ϕ appearing in (A-8).

The following manipulations serve to transfer the differential operator on ϕ in (A-12) to $\underset{\sim}{W}_{mi}^p$. If S is closed,

$$\iint_S \nabla_{s} \cdot (\phi \underset{\sim}{W})\, ds = 0 \tag{A-14}$$

where $\underset{\sim}{W}$ denotes $\underset{\sim}{W}_{mi}^p$. If S has an edge, the surface divergence theorem yields

$$\iint_S \nabla_{s} \cdot (\phi \underset{\sim}{W})\, ds = \int_C \hat{t} \cdot \phi \underset{\sim}{W}\, dc$$

where C is the path of the edge. Hence, with $\underset{\sim}{W}$ chosen such that $\hat{t} \cdot \underset{\sim}{W} = 0$ along the edge, (A-14) holds whether S is open or closed.

The representation

$$\nabla_{s} \cdot \underset{\sim}{W} = \frac{1}{\rho} \frac{\partial}{\partial t} (\rho\, \underset{\sim}{W} \cdot \hat{t}) + \frac{1}{\rho} \frac{\partial}{\partial \phi} (\underset{\sim}{W} \cdot \hat{\phi}) \tag{A-15}$$

of the surface divergence and the definition

$$\nabla_{s} \phi = \hat{t}\, \frac{\partial \phi}{\partial t} + \hat{\phi}\, \frac{\partial \phi}{\rho \partial \phi} \tag{A-16}$$

of the surface gradient imply that

$$\nabla_{s} \cdot (\phi \underset{\sim}{W}) = \phi \nabla_{s} \cdot \underset{\sim}{W} + \underset{\sim}{W} \cdot \nabla_{s} \phi \tag{A-17}$$

The surface gradient of ϕ in (A-17) can be replaced by the ordinary three-dimensional gradient of ϕ because (A-16) is the component of the three-dimensional gradient tangential to S and $\underset{\sim}{W}$ is tangential to S. Substitution of (A-17) into (A-14) and then (A-14) into (A-12) yields

$$Z^{pq}_{mnij} = j\omega \iint_S \left(\underset{\sim}{W}^p_{mi} \cdot \underset{\sim}{A}(\underset{\sim}{J}^q_{nj}) + \sigma^p_{mi} \, \Phi(\underset{\sim}{J}^q_{nj}) \right) ds \tag{A-18}$$

where

$$\sigma^p_{mi} = -\frac{1}{j\omega} \underset{\sim}{\nabla}_s \cdot \underset{\sim}{W}^p_{mi} \tag{A-19}$$

Since, as shown in Appendix B of Reference 1, (A-18) is zero for $m \neq n$, (A-11) reduces to

$$\begin{bmatrix} [Z^{tt}_n] & [Z^{t\phi}_n] \\ [Z^{\phi t}_n] & [Z^{\phi\phi}_n] \end{bmatrix} \begin{bmatrix} \vec{I}^t_n \\ \vec{I}^\phi_n \end{bmatrix} = \begin{bmatrix} \vec{V}^t_n \\ \vec{V}^\phi_n \end{bmatrix}, \quad n=0, \pm1, \pm2, \ldots \tag{A-20}$$

where $[Z^{pq}_n]$ is $[Z^{pq}_{nn}]$ of (A-18). It also is shown in Appendix B of Reference 1 that the elements of $[Z^{pq}_n]$ are given by

$$Z^{tt}_{nij} = j\eta \int dt \int dt' \left(k^2 \rho f^t_i(t) \; \rho' f^t_j(t') \; (G_5 \sin v \sin v' + G_4 \cos v \cos v') \right.$$

$$\left. - \frac{\partial}{\partial t} (\rho f^t_i(t)) \left(\frac{\partial}{\partial t'}, \; \rho' f^t_j(t')\right) G_4 \right) \tag{A-21}$$

$$Z^{\phi t}_{nij} = -\eta \int dt \; \rho f^\phi_i(t) \int dt' \left(k^2 \rho' f^t_j(t') \; G_6 \sin v' + \frac{n}{\rho} \frac{\partial}{\partial t'} (\rho' f^t_j(t')) \; G_4 \right) \tag{A-22}$$

$$Z^{t\phi}_{nij} = \eta \int dt \int dt' \; \rho' f^\phi_j(t') \left(k^2 \rho f^t_i(t) \; G_6 \sin v + \frac{n}{\rho'} \frac{\partial}{\partial t} (\rho f^t_i(t)) \; G_4 \right) \tag{A-23}$$

$$Z^{\phi\phi}_{nij} = j\eta \int dt \; \rho f^\phi_i(t) \int dt' \rho' f^\phi_j(t') \left(k^2 G_5 - \frac{n^2}{\rho\rho'} \; G_4 \right) \tag{A-24}$$

where η is the wave impedance, $\sqrt{\mu/\varepsilon}$, v is the angle between the tangent to the generating curve and the z axis,

$$G_4 = \int_0^{\pi} d\phi' \frac{e^{-jkR}}{kR} \cos(n\phi') \tag{A-25}$$

$$G_5 = \int_0^{\pi} d\phi' \frac{e^{-jkR}}{kR} \cos\phi' \cos(n\phi') \tag{A-26}$$

$$G_6 = \int_0^{\pi} d\phi' \frac{e^{-jkR}}{kR} \sin\phi' \sin(n\phi') \tag{A-27}$$

and

$$R = \sqrt{(\rho-\rho')^2 + (z-z')^2 + 4\rho\rho' \sin^2(\frac{\phi'}{2})}$$

Here, ρ, z, and v depend on t while ρ', z', and v' depend on t'.

To evaluate (A-21) through (A-24), $\rho f_i^t(t)$ is defined as a four-impulse approximation to a triangle function in the following manner. Letting $t = (\rho,z)$, denote that ρ and z are cylindrical coordinates of the point t, an odd number greater than or equal to 5 of consecutive points $t = (\rho,z) = \bar{t}_i = (\bar{\rho}_i, \bar{z}_i)$, $i = 1, 2, \ldots P$ on the generating curve of the body of revolution such that $(\bar{\rho}_1, \bar{z}_1)$ and $(\bar{\rho}_P, \bar{z}_P)$ are the poles. If the body of revolution has no poles because the generating curve closes upon itself, as with a torus, then two points must be overlapped such that

$$(\bar{\rho}_{P-1}, \bar{z}_{P-1}) = (\bar{\rho}_1, \bar{z}_1) \quad \text{and} \quad (\bar{\rho}_P, \bar{z}_P) = (\bar{\rho}_2, \bar{z}_2)$$

The generating curve is approximated by drawing straight lines between the points $(\bar{\rho}_i, \bar{z}_i)$, $i = 1, 2, \ldots P$ and defining points

$$t = t_i = (\rho_i, z_i) = \frac{\bar{\rho}_i + \bar{\rho}_{i+1}}{2}, \frac{\bar{z}_i + \bar{z}_{i+1}}{2} \tag{A-28}$$

on this approximate generating curve. The length, d_i, of the interval centered about t_i is given by

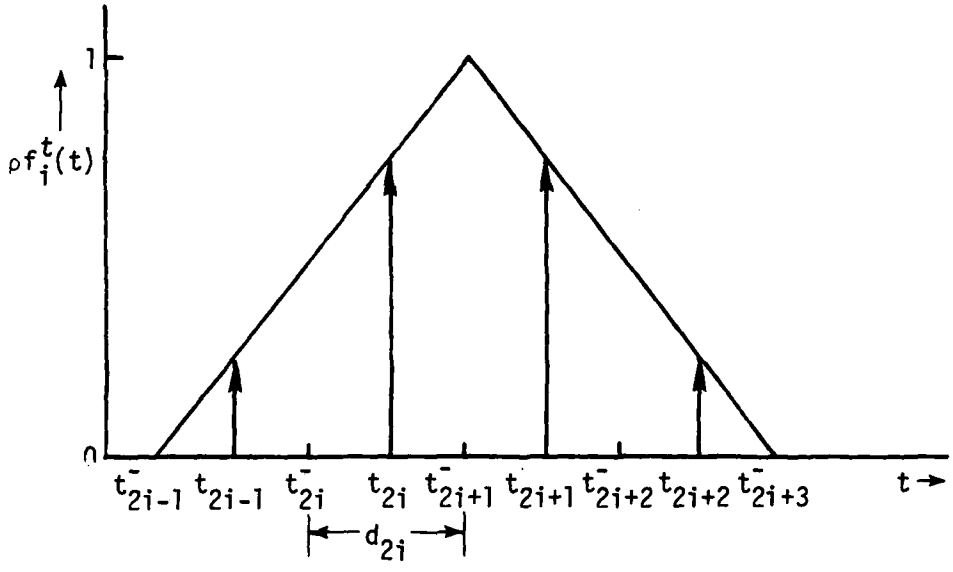

Figure A-3. Triangle Function (Solid) and Four Impulse Approximation (Arrows)

$$d_i = \sqrt{(\rho^-_{i+1} - \rho^-_i)^2 + (z^-_{i+1} - z^-_i)^2} \tag{A-29}$$

In terms of coefficients T_{p+4i-4} defined by

$$\begin{aligned}
T_{4i-3} &= \frac{kd^2_{2i-1}}{2(d_{2i-1} + d_{2i})} \\
T_{4i-2} &= \frac{k(d_{2i-1} + \frac{1}{2} d_{2i})d_{2i}}{d_{2i-1} + d_{2i}} \\
T_{4i-1} &= \frac{k(d_{2i+2} + \frac{1}{2} d_{2i+1})d_{2i+1}}{d_{2i+1} + d_{2i+2}} \\
T_{4i} &= \frac{kd^2_{2i+2}}{2(d_{2i+1} + d_{2i+2})}
\end{aligned} \tag{A-30}$$

one constructs

$$\rho f^t_i(t) = \frac{1}{k} \sum_{p=1}^{4} T_{p+4i-4}\ \delta(t-t_{p+2i-2}) \tag{A-31}$$

where $\delta(t)$ is the unit impulse function. The right-hand side of (A-31) is the desired four-impulse approximation to a triangle function (Figure A-3).

The $\rho f^\phi_i(t)$ are chosen equal to $\rho f^t_i(t)$ except at an edge where the ϕ component of surface current approaches infinity; therefore, the $\rho f^\phi_i(t)$ functions nearest edges are chosen as ramp functions (Figure A-4). A four-impulse approximation results in

$$\rho f^\phi_i(t) = \frac{1}{k} \sum_{p=1}^{4} TR_{p+4i-4}\ \delta(t-t_{p+2i-2}) \tag{A-32}$$

where $TR_{p+4i-4} = T_{p+4i-4}$ except for TR_1 and TR_2 if an edge exists at the beginning of the generating curve or for TR_{4ne-1} and TR_{4ne} if an edge exists at the end of the generating curve where ne = number of ρf^ϕ_i traversing the generating curve. For a beginning edge,

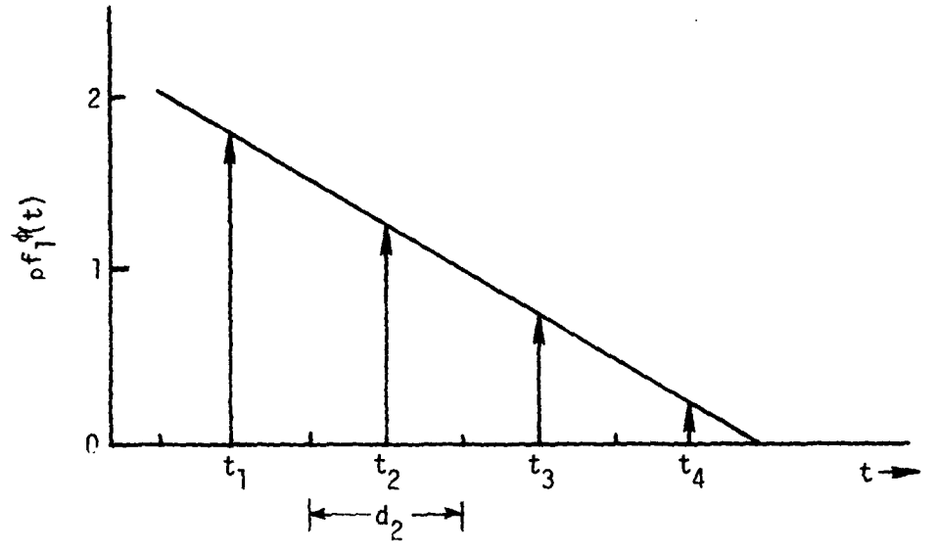

a. Leading Edge

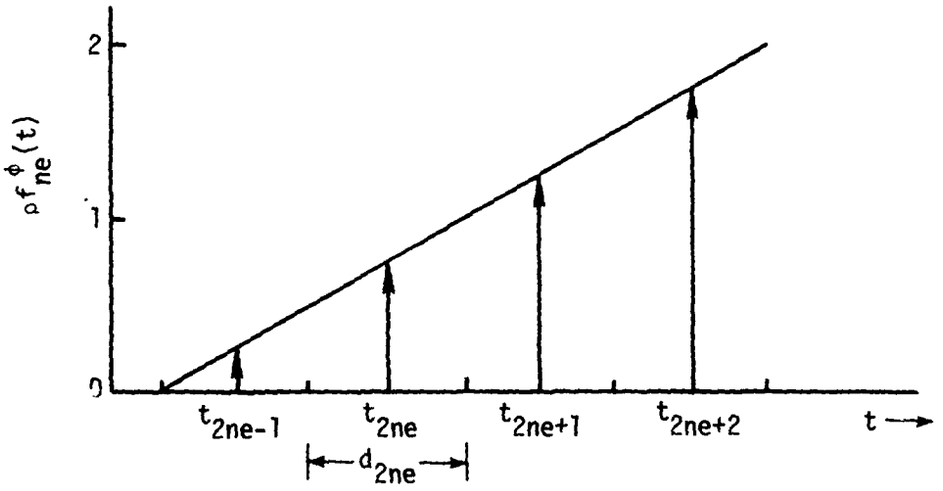

b. Terminating Edge

Figure A-4. Triangle Function (Solid) and Four Impulse Approximation (Arrows) for ϕ Directed Current

$$TR_1 = 2kd_1 - T_1$$

$$TR_2 = 2kd_2 - T_2 \qquad \text{(A-33)}$$

For an end edge,

$$TR_{4ne-1} = 2kd_{ng-1} - T_{4ne-1}$$

$$TR_{4ne} = 2kd_{ng} - T_{4ne} \qquad \text{(A-34)}$$

where ng = number of segments traversing the generating curve.

For $\frac{d}{dt}(\rho f_i^t(t))$, the four impulse approximation

$$\frac{d}{dt}(\rho f_i(t)) = \sum_{p=1}^{4} T'_{p+4i-4}\,\delta(t-t_{p+2i-2}) \qquad \text{(A-35)}$$

to the derivative of the triangle function of Figure A-3 is chosen. Figure A-5 illustrates A-35.

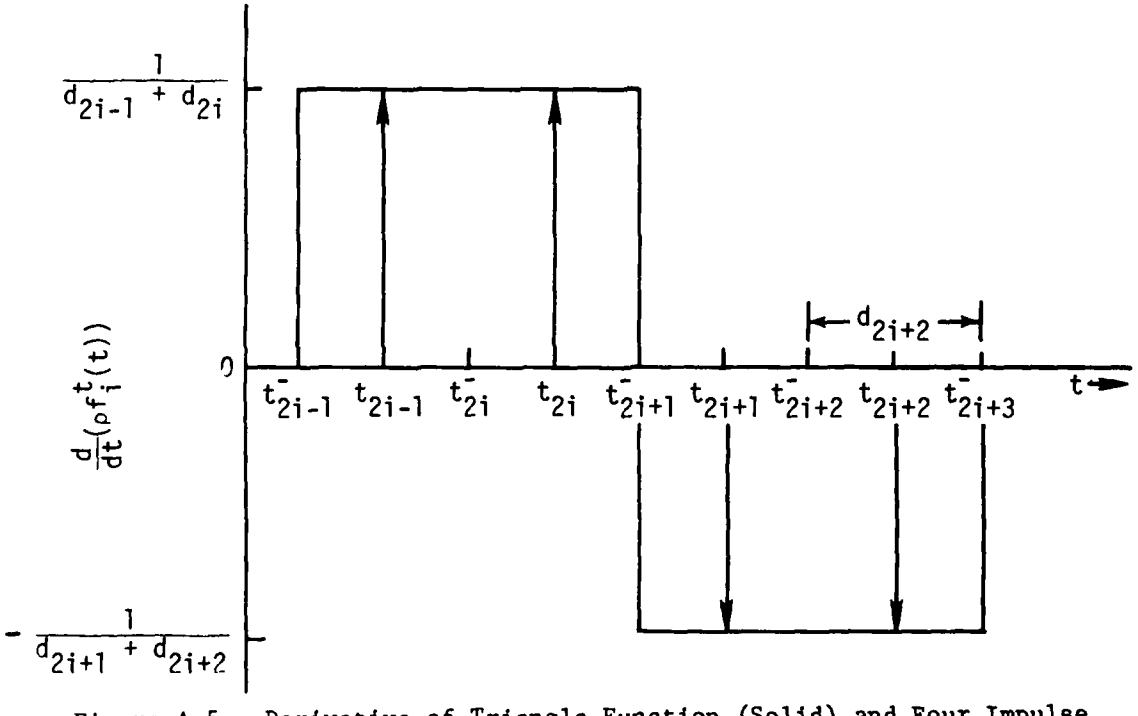

Figure A-5. Derivative of Triangle Function (Solid) and Four Impulse Approximation (Arrows)

The coefficients T'_{p+4i-4} appearing in (A-35) are given by

$$T'_{4i-3} = \frac{d_{2i-1}}{d_{2i-1} + d_{2i}}$$

$$T'_{4i-2} = \frac{d_{2i}}{d_{2i-1} + d_{2i}} \qquad \text{(A-36)}$$

$$T'_{4i-1} = \frac{-d_{2i+1}}{d_{2i+1} + d_{2i+2}}$$

$$T'_{4i} = \frac{-d_{2i+2}}{d_{2i+1} + d_{2i+2}}$$

where d_i is defined by (A-29).

Substituting (A-31), (A-32), and (A-35) into (A-21) through (A-24) yields

$$Z^{tt}_{nij} = j\eta \sum_{p=1}^{4}\sum_{q=1}^{4} (T_p, T_q, (G_5 \sin v_i, \sin v_j, + G_4 \cos v_i, \cos v_j,) - T'_p, T'_q, G_4) \qquad \text{(A-37)}$$

$$Z^{\phi t}_{nij} = -\eta \sum_{p=1}^{4}\sum_{q=1}^{4} (TR_p, T_q, (G_6 \sin v_j, + \frac{n}{k\rho_i}, TR_p, T'_q, G_4) \qquad \text{(A-38)}$$

$$Z^{t\phi}_{nij} = \eta \sum_{p=1}^{4}\sum_{q=1}^{4} (T_p, TR_q, G_6 \sin v_i, + \frac{n}{k\rho_j}, T'_p, TR_q, G_4) \qquad \text{(A-39)}$$

$$Z^{\phi\phi}_{nij} = j\eta \sum_{p=1}^{}\sum_{q=1}^{} TR_p, TR_q, (G_5 - \frac{n^2}{k^2\rho_i,\rho_j,} G_4) \qquad \text{(A-40)}$$

where

$$p' = p + 4i - 4$$

$$q' = q + 4j - 4 \qquad \text{(A-41)}$$

$$i' = p + 2i - 2$$
$$j' = q + 2j - 2 \qquad \text{(A-41)}$$

The subscript i' denotes evaluation at $t_{i'}$. The subscript j' denotes evaluation at $t_{j'}$. G_4, G_5, and G_6 are given by (A-25), (A-26), and (A-27) in which R is evaluated at $t = t_{i'}$, $t' = t_{j'}$, which, in terms of cylindrical coordinates, is at ρ, z, ρ', $z' = \rho_{i'}$, $z_{i'}$, $\rho_{j'}$, $z_{j'}$. If i' = j', R is replaced by an equivalent distance, R_e, given by

$$R_e = \sqrt{(d_{i'}/4)^2 + 4\rho_{i'}^2 \sin^2(\phi'/2)} \qquad \text{(A-42)}$$

(A-42) may be obtained by displacing the field point a distance $d_{i'}/4$ perpendicular to the plane of the source loop. Now, $d_{i'}/4$ is the equivalent radius [2] of a flat strip whose width is $d_{i'}$. (A-42) also can be obtained by averaging R^2 for field points displaced a distance $d_{i'}/4$ in either direction along the approximate generating curve from the source loop.

An N_ϕ point Gaussian quadrature formula is used to calculate the integrals G_4, G_5, and G_6 defined by (A-25), (A-26), and (A-27). According to this quadrature formula,

$$\int_0^\pi f(\phi')\, d\phi' = \frac{\pi}{2} \sum_{k=1}^{N_\phi} A_k\, f\left(\frac{\pi}{2}(x_k + 1)\right) \qquad \text{(A-43)}$$

where $f(\phi')$ is the function being integrated and x_k and A_k are constants tabulated by Krylov [3]. In (A-43), the multiplier, $\frac{\pi}{2}$, and argument, $\frac{\pi}{2}(x_k + 1)$, instead of just x_k are due to the transformation of Krylov's interval from -1 to 1 into the interval from 0 to π.

Since replacement of i, j, p, and q in (A-41) with j, i, q, and p, respectively, implies replacement of i', j', p', and q' in (A-37) through (A-40) with j', i', and q', and p', respectively, and since G_4, G_5, and G_6 are symmetric in i' and j', it is evident that

$$Z_{nij}^{tt} = Z_{nji}^{tt} \qquad \text{(A-44)}$$

$$Z^{\phi t}_{nij} = - Z^{t\phi}_{nji}$$

$$Z^{\phi\phi}_{nij} = Z^{\phi\phi}_{nji} \qquad \text{(A-44)}$$

An efficient method of computing (A-34) through (A-40) that takes advantage of (A-44) is employed in the computer code described in [4].

2. PLANE WAVE EXCITATION

The n^{th} mode generalized voltage vectors, $\vec{V}^{t}_{n}$ and $\vec{V}^{\phi}_{n}$, are matrix column vectors with elements defined by (A-13) (with m replaced by n). For plane wave excitation, (A-13) becomes, after substitution from (A-1), (A-2), and (A-10),

$$V^{t\theta}_{ni} = \int dt\ \rho f^{t}_{i}(t) \int_{0}^{2\pi} d\phi\ (\hat{t}\cdot\hat{\theta}_{e})\ e^{-j(\underset{\sim}{k}_{e}\cdot\underset{\sim}{r}+n\phi)}$$

$$V^{\phi\theta}_{ni} = \int dt\ \rho f^{\phi}_{i}(t) \int_{0}^{2\pi} d\phi\ (\hat{\phi}\cdot\hat{\theta}_{e})\ e^{-j(\underset{\sim}{k}_{e}\cdot\underset{\sim}{r}+n\phi)} \qquad \text{(A-45)}$$

$$V^{t\phi}_{ni} = \int dt\ \rho f^{t}_{i}(t) \int_{0}^{2\pi} d\phi\ (\hat{t}\cdot\hat{\phi}_{e})\ e^{-j(\underset{\sim}{k}_{e}\cdot\underset{\sim}{r}+n\phi)}$$

$$V^{\phi\phi}_{ni} = \int dt\ \rho f^{\phi}_{i}(t) \int_{0}^{2\pi} d\phi\ (\hat{\phi}\cdot\hat{\phi}_{e})\ e^{-j(\underset{\sim}{k}_{e}\cdot\underset{\sim}{r}+n\phi)}$$

where the second superscript on V is θ for the incident field $\underset{\sim}{E}^{e}$ given by (A-1) and ϕ for $\underset{\sim}{E}^{e}$ given by (A-2).

With a view toward evaluation of (A-45), it can be seen from Figures (A-2), (A-6), and (A-7) that

$$\hat{t}\cdot\hat{\theta}_{e} = -\sin\theta_{e}\cos v + \cos\theta_{e}\sin v\cos\phi$$

$$\phi\cdot\theta_{e} = -\cos\theta_{e}\sin\phi \qquad \text{(A-46)}$$

$$\hat{t}\cdot\hat{\theta}_{e} = \sin v\sin\phi$$

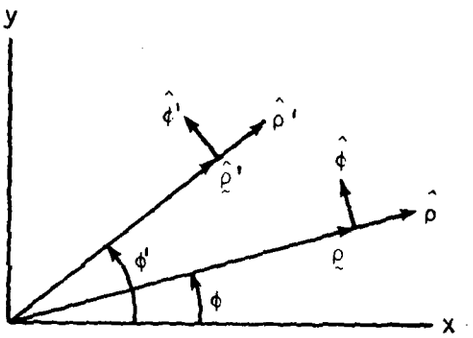

Figure A-6. Unit Vectors $\hat{\rho}$, $\hat{\phi}$, $\hat{\rho}'$, and $\hat{\phi}'$ in xy Plane

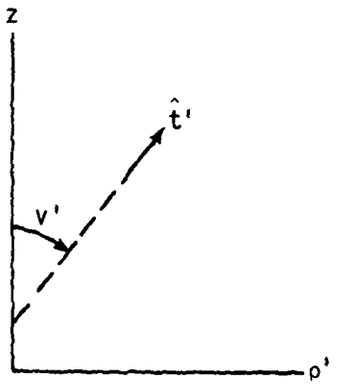

Figure A-7. Unit Vector $\hat{t}'$ in $\rho'z$ Plane

$$\hat{\phi}\cdot\hat{\phi}_e = \cos\phi$$

$$\underset{\sim}{k}_e\cdot\underset{\sim}{r} = -kz\cos\theta_e - k\rho\sin\theta_e\cos\phi \tag{A-46}$$

The substitution (A-46), (A-31), and (A-32) into (A-45) and the integral formula

$$J_n(k\rho\sin\theta_e) = \frac{j^{-n}}{2\pi}\int_0^{2\pi} e^{j(k\rho\sin\theta_e\cos\phi + n\phi)}\,d\phi \tag{A-47}$$

deduced from (9.1.21) of [5] for Bessel functions, yields

$$V_{ni}^{t\theta} = \frac{\pi j^n}{k}\sum_{p=1}^{4} T_{p+4i-4}(-2J_n\sin\theta_e\cos v + j\,(J_{n+1} - J_{n-1})\cos\theta_e\sin v)e^{jkz\cos\theta_e}$$

$$V_{ni}^{\phi\theta} = \frac{\pi j^n}{k}\sum_{p=1}^{4} T_{p+4i-4}(J_{n+1} + J_{n-1})\cos\theta_e\, e^{jkz\cos\theta_e} \tag{A-48}$$

$$V_{ni}^{t\phi} = -\frac{\pi j^n}{k}\sum_{p=1}^{4} T_{p+4i-4}(J_{n+1} + J_{n-1})\sin v\, e^{jkz\cos\theta_e}$$

$$V_{ni}^{\phi\phi} = \frac{\pi j^{n+1}}{k}\sum_{p=1}^{4} T_{p+4i-4}(J_{n+1} - J_{n-1})\, e^{jkz\cos\theta_e}$$

where

$$J_n = J_n(k\rho\sin\theta_e) \tag{A-49}$$

In (A-48), ρ, z, and v are to be evaluated at $t = t_{p+2i-2}$.

3. SCATTERING CURRENT

The solution to (A-20) yields the electric surface current coefficients I^t_{nj}, I^ϕ_{nj} for each BOR mode n. The expression (A-8) for the corresponding surface current can be simplified, for plane wave excitation, by combining the n and -n terms. The substitution (A-9) into (A-8) yields

$$\underset{\sim}{J}^q = \sum_{n=-\infty}^{\infty} e^{jn\phi} \{(\tilde{f}^t \vec{I}^{tq}_n)\hat{t} + (\tilde{f}^\phi \vec{I}^{\phi q}_n)\hat{\phi}\} \qquad \text{(A-50)}$$

where $\tilde{f}^t$ is the transpose of the column vector $\vec{f}^t$ of the $f^t_j(t)$, $\tilde{f}^\phi$ is the transpose of the column vector $\vec{f}^\phi$ of the $f^\phi_j(t)$, and $\vec{I}^{tq}_n$ and $\vec{I}^{\phi q}_n$ are column vectors of the coefficients I^t_{nj} and I^ϕ_{nj} respectively. The additional superscript, q, is either θ or ϕ, depending on whether the incident electric field is θ polarized as in (A-1) or ϕ polarized as in (A-2). The column vectors, $\vec{I}^{tq}_n$ and $\vec{I}^{\phi q}_n$, are obtained by solving the matrix equation (A-20) with the additional superscript q on the column vectors therein to denote the polarization of the incident electric field.

Inspection of (A-21) through (A-27) reveals that

$$\begin{bmatrix} \begin{bmatrix} Z^{tt}_{-n} \end{bmatrix} & \begin{bmatrix} Z^{t\phi}_{-n} \end{bmatrix} \\ \begin{bmatrix} Z^{\phi t}_{-n} \end{bmatrix} & \begin{bmatrix} Z^{\phi\phi}_{-n} \end{bmatrix} \end{bmatrix} = \begin{bmatrix} \begin{bmatrix} Z^{tt}_{n} \end{bmatrix} & \begin{bmatrix} -Z^{t\phi}_{n} \end{bmatrix} \\ \begin{bmatrix} -Z^{\phi t}_{n} \end{bmatrix} & \begin{bmatrix} Z^{\phi\phi}_{n} \end{bmatrix} \end{bmatrix} \qquad n = 0, 1, 2, \ldots \qquad \text{(A-51)}$$

It is apparent from (A-48) that

$$\begin{bmatrix} \vec{V}^{t\theta}_{-n} & \vec{V}^{t\phi}_{-n} \\ \vec{V}^{\phi\theta}_{-n} & \vec{V}^{\phi\phi}_{-n} \end{bmatrix} = \begin{bmatrix} \vec{V}^{t\theta}_{n} & -\vec{V}^{t\phi}_{n} \\ -\vec{V}^{\phi\theta}_{n} & \vec{V}^{\phi\phi}_{n} \end{bmatrix} \qquad n = 0, 1, 2, \ldots \qquad \text{(A-52)}$$

Since the property (A-51) survives matrix inversion, it is evident from (A-20) and (A-52) that

$$\begin{bmatrix} \vec{I}^{t\theta}_{-n} & \vec{I}^{t\phi}_{-n} \\ \vec{I}^{\phi\theta}_{-n} & \vec{I}^{\phi\phi}_{-n} \end{bmatrix} = \begin{bmatrix} \vec{I}^{t\theta}_{n} & -\vec{I}^{t\phi}_{n} \\ -\vec{I}^{\phi\theta}_{n} & \vec{I}^{\phi\phi}_{n} \end{bmatrix} \qquad n = 0, 1, 2, \ldots \tag{A-53}$$

In view of (A-53), (A-50) becomes

$$\underset{\sim}{J}^{\theta} = (\tilde{f}^{t}\ \vec{I}^{t\theta}_{0})\ \hat{t} + \sum_{n=1}^{\infty} \{2(\tilde{f}^{t}\ \vec{I}^{t\theta}_{n})\ \hat{t}\cos(n\phi) + 2j(\tilde{f}^{\phi}\ \vec{I}^{\phi\theta}_{n})\ \hat{\phi}\sin(n\phi)\}$$

$$\underset{\sim}{J}^{\phi} = (\tilde{f}^{\phi}\ \vec{I}^{\phi\phi}_{0})\ \hat{\phi} + \sum_{n=1}^{\infty} \{2j(\tilde{f}^{t}\ \vec{I}^{t\phi}_{n})\ \hat{t}\sin(n\phi) + 2(\tilde{f}^{\phi}\ \vec{I}^{\phi\phi}_{n})\ \hat{\phi}\cos(n\phi)\} \tag{A-54}$$

where $\tilde{f}^{t}$ and $\tilde{f}^{\phi}$ are row vectors of the $f^{t}_{j}(t)$ and $f^{\phi}_{j}(t)$, respectively. If $\rho f^{t}_{j}(t)$ and $pf^{\phi}_{j}(t)$ are the triangle functions themselves, rather than the four-impulse approximations (A-31) and (A-32) to the triangle functions, then

$$\underset{\sim}{J}^{\theta}\Big|_{t=t^{-}_{2i+1}} = \frac{I^{t\theta}_{0i}\ \hat{t} + \sum_{n=1}^{\infty} \{2I^{t\theta}_{ni}\ \hat{t}\cos(n\phi) + 2j\ I^{\phi\theta}_{ni}\ \hat{\phi}\sin(n\phi)\}}{\rho^{-}_{2i+1}}$$

$$\underset{\sim}{J}^{\phi}\Big|_{t=t^{-}_{2i+1}} = \frac{I^{\phi\phi}_{0i}\ \hat{\phi} + \sum_{n=1}^{\infty} \{2jI^{t\phi}_{ni}\ \hat{t}\sin(n\phi) + 2I^{\phi\phi}_{ni}\ \hat{\phi}\cos(n\phi)\}}{\rho^{-}_{2i+1}} \tag{A-55}$$

4. NEAR E-FIELD

Near E-fields are computed in a manner similar to that described by Bevensee [6]. The E-field, $\underset{\sim}{E}^s_n$, radiated by the n^{th} mode of BOR current $\underset{\sim}{J}_n$, along a circular path concentric with the BOR axis is sought. This path is thickened into a ribbon of surface area $\bar{S}$ (Figure A-8). A test surface current

$$\underset{\sim}{\bar{J}}_n = \underset{\sim}{\bar{J}}^t_n + \underset{\sim}{\bar{J}}^\phi_n \tag{A-56}$$

having $e^{-jn\phi}$ circumferential variation, resides on $\bar{S}$ where the t component, $\underset{\sim}{\bar{J}}^t_n$, lies in the plane formed by the BOR generating curve and BOR axis and $\underset{\sim}{\bar{J}}^\phi_n$ is the ϕ-directed component. By reciprocity [7], the t and ϕ components of $\underset{\sim}{E}^s_n(\underset{\sim}{J}_n)$ satisfy

$$\iint_{\bar{S}} \underset{\sim}{E}^s_n(\underset{\sim}{J}_n)\cdot\underset{\sim}{\bar{J}}^a_n \, ds = \iint_S \underset{\sim}{\bar{E}}_n(\underset{\sim}{\bar{J}}^a_n)\cdot\underset{\sim}{J}_n \, ds \tag{A-57}$$

where a = t or ϕ and $\underset{\sim}{\bar{E}}_n$ is the E-field radiated by $\underset{\sim}{\bar{J}}^a_n$.

With $\underset{\sim}{J}_n$ given by the n^{th} mode terms in the summation (A-8), the right-hand side of (A-57) becomes

$$\iint_S \underset{\sim}{\bar{E}}_n(\underset{\sim}{\bar{J}}^a_n)\cdot\underset{\sim}{J}_n \, ds = \tilde{\bar{Z}}^{at}_n \, \vec{\bar{I}}^t_n + \tilde{\bar{Z}}^{a\phi} \, \vec{\bar{I}}^\phi_n \tag{A-58}$$

where $\vec{\bar{I}}^t_n$ and $\vec{\bar{I}}^\phi_n$ are defined following (A-12) and $\tilde{\bar{Z}}^{at}_n$ and $\tilde{\bar{Z}}^{a\phi}_n$ are matrix row vectors. The i^{th} elements of $\tilde{Z}^{at}_n$ and $\tilde{Z}^{a\phi}_n$ are

$$\begin{aligned} \bar{Z}^{ab}_{ni} &= \iint_S \underset{\sim}{\bar{E}}_n(\underset{\sim}{\bar{J}}^a_n)\cdot\underset{\sim}{J}^b_{ni} \, ds \\ &= -\iint_S (j\omega \underset{\sim}{A}(\underset{\sim}{\bar{J}}^a_n) + \nabla\Phi(\underset{\sim}{\bar{J}}^a_n))\cdot\underset{\sim}{J}^b_{ni} \, ds \end{aligned} \tag{A-59}$$

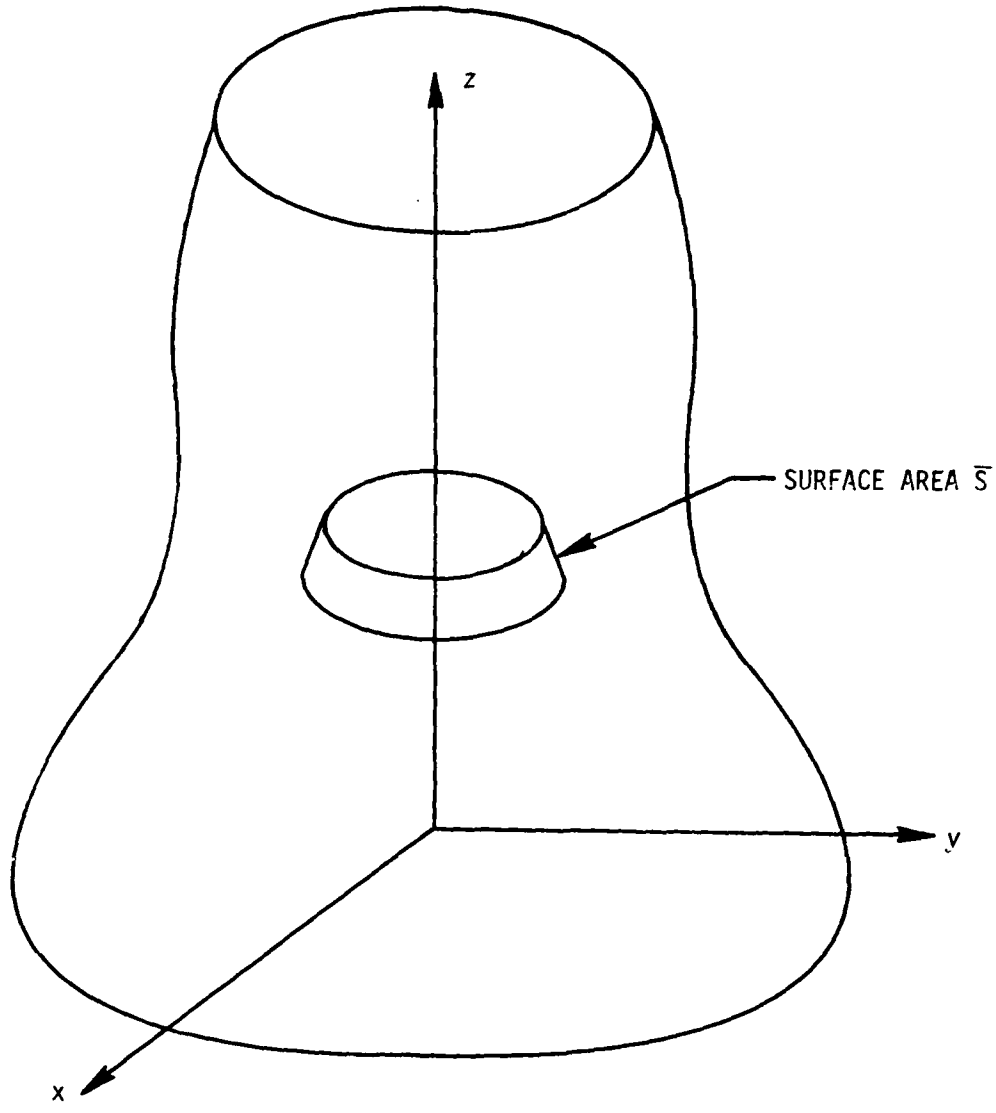

Figure A-8. Body of Revolution with Near-Field Test Ribbon

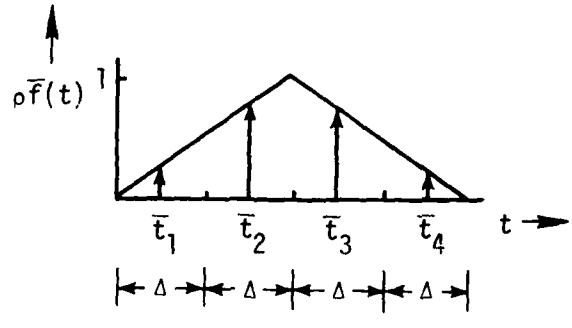

Figure A-9. Near-Field Test Ribbon Triangle Function (Solid) and Four-Impulse Approximation (Arrows)

where a = t or ϕ and b = t or ϕ, and the vector and scalar potential functions, A and Φ, are given by (A-5) and (A-6

Let $\bar{J}^{t}_{n}$ and $\bar{J}^{\phi}_{n}$ be defined b·

$$\bar{J}^{t}_{n} = \hat{t}\ \bar{f}(t)\ e^{-jn\phi} \tag{A-60}$$

$$\bar{J}^{\phi}_{n} = \hat{\phi}\ \bar{f}(t)\ e^{-jn\phi} \tag{A-61}$$

where $\rho\bar{f}(t)$ is the "triangular" function shown in Figure A-9. The right-hand side of (A-59) then is within a minus sign of (A-12) if m and n in (A-12) are each replaced by -n, and $\underset{\sim}{f}^{t}_{j}(t)$ and $\underset{\sim}{f}^{\phi}_{j}(t)$ are each replaced by $\bar{f}(t)$. In this comparison of (A-59) with (A-12), the tϕ and ϕt terms on the left-hand side of (A-12) are reversed from these of (A-15); therefore, the four-impulse approximations to $\rho\bar{f}(t)$ and $\frac{d}{dt}(\rho\bar{f}(t))$ are given by

$$\rho\bar{f}(t) = \frac{1}{k}\sum_{p=1}^{4}\bar{T}_{p}\ \delta(t - (p - \tfrac{1}{2})\Delta) \tag{A-62}$$

$$\frac{d}{dt}(\rho\bar{f}(t)) = \sum_{p=1}^{4}\bar{T}'_{p}\ \delta(t - (p - \tfrac{1}{2})\Delta)$$

where

$$\bar{T}_1 = \bar{T}_4 = \frac{k\Delta}{4}$$

$$\bar{T}_2 = \bar{T}_3 = \frac{k3\Delta}{4}$$

$$\bar{T}'_1 = \bar{T}'_2 = \frac{1}{2}$$

$$\bar{T}'_3 = \bar{T}'_4 = -\frac{1}{2}$$

and comparison with (A-37) through (A-40) and (A-25) through (A-27) yields

$$\bar{Z}^{tt}_{ni} = -j\eta \sum_{p=1}^{4} \sum_{q=1}^{4} \{T_p, \bar{T}_q \, (G_5 \sin v_i, \sin \bar{v} + G_4 \cos v_i, \cos \bar{v}) - T'_p, T'_q \, G_4\} \tag{A-63}$$

$$\bar{Z}^{t\phi}_{ni} = \eta \sum_{p=1}^{4} \sum_{q=1}^{4} \{TR_p, T_q \, G_6 \sin \bar{v} - \frac{n}{k\rho_i} TR_p, \bar{T}'_q \, G_4\} \tag{A-64}$$

$$\bar{Z}^{\phi t}_{ni} = -\eta \sum_{p=1}^{4} \sum_{q=1}^{4} \{T_p, \bar{T}_q \, G_6 \sin v_i, - \frac{n}{k\bar{\rho}_q} T'_p, \bar{T}_q \, G_4\} \tag{A-65}$$

$$\bar{Z}^{\phi\phi}_{ni} = -j\eta \sum_{p=1}^{4} \sum_{q=1}^{4} \{TR_p, \bar{T}_q \, (G_5 - \frac{n^2}{k^2 \rho_i, \bar{\rho}_q} G_4) \tag{A-66}$$

In (A-63) to (A-66)

$$G_4 = \int_0^{\pi} d\phi' \, \frac{e^{-jkR}}{kR} \cos (n\phi') \tag{A-67}$$

$$G_5 = \int_0^{\pi} d\phi' \, \frac{e^{-jkR}}{kR} \cos \phi' \cos (n\phi') \tag{A-68}$$

$$G_6 = \int_0^{\pi} d\phi' \, \frac{e^{-jkR}}{kR} \sin \phi' \sin (n\phi') \tag{A-69}$$

$$R = \sqrt{(\rho_i, - \bar{\rho}_q)^2 + (z_i, - \bar{z}_q)^2 + 4\rho_i \bar{\rho}_q \sin^2 (\frac{\phi'}{2})} \tag{A-70}$$

$$p' = p + 4i - 4$$

$$i' = p + 2i - 2$$

$\bar{v}$ is the angle between the t coordinate of the test surface, $\bar{S}$, and the z axis; $\bar{\rho}_q$ and $\bar{z}_q$ are the ρ, z coordinates of $\bar{t}_q$ in Figure A-9.

Due to the rotational symmetry, the $e^{jn\phi}$ variation of J_n (Equation (A-9)) implies the same $e^{jn\phi}$ variation of $E^s_n(J_n)$; i.e., $E^s_n(J_n)$ may be written

$$E^s_n(J_n) = \hat{t}E^t_n e^{jn\phi} + \hat{\phi}E^\phi_n e^{jn\phi} \tag{A-71}$$

where E^t_n and E^ϕ_n are ϕ independent. If E^s_n is approximately uniform over the width of $\bar{S}$, the left-hand side of (A-57) becomes approximately

$$\iint_{\bar{S}} E^s_n(J_n)\cdot\bar{J}^a_n \, ds = E^a_n \int_0^{4\Delta}\int_0^{2\pi} \bar{f}(t)\, \rho \, d\phi \, dt$$

$$= E^a_n \, 4\pi\Delta \tag{A-72}$$

where a = t or ϕ. Equations (A-57), (A-58), and (A-72) yield

$$E^a_n = \frac{1}{4\pi\Delta}\left(\tilde{Z}^{at}_n \vec{I}^t_n + \tilde{Z}^{a\phi}_n \vec{I}^\phi_n\right) \tag{A-73}$$

The $\hat{t}$ and ϕ components of the E-field E^s radiated by the BOR surface current are expressed as

$$\hat{t}\cdot E^s = E^t_0 + \sum_{n=1}^{\infty}\left(E^t_n e^{jn\phi} + E^t_{-n} e^{-jn\phi}\right)$$

$$\hat{\phi}\cdot E^s = E^\phi_0 + \sum_{n=1}^{\infty}\left(E^\phi_n e^{jn\phi} + E^\phi_{-n} e^{-jn\phi}\right) \tag{A-74}$$

where E_n^t and E_n^ϕ are given by (A-73). The positive and negative "n" modes -- e.g., E_n^t and E_{-n}^t -- can be combined, as shown below, for each polarization, θ and ϕ , of incident plane wave (A-1) and (A-2). In the following development, a second superscript on E_n^t, E_n^ϕ, $\vec{I}_n^t$, or $\vec{I}_n^\phi$ refers to this incident field polarization.

It is apparent from (A-63) through (A-69) that

$$\begin{aligned} \tilde{\tilde{Z}}_{-n}^{tt} &= \tilde{\tilde{Z}}_n^{tt} \\ \tilde{\tilde{Z}}_{-n}^{t\phi} &= -\tilde{\tilde{Z}}_n^{t\phi} \\ \tilde{\tilde{Z}}_{-n}^{\phi t} &= -\tilde{\tilde{Z}}_n^{\phi t} \\ \tilde{\tilde{Z}}_{-n}^{\phi\phi} &= \tilde{\tilde{Z}}_n^{\phi\phi} \end{aligned} \qquad \text{(A-75)}$$

From (A-73), (A-53), and (A-75), therefore,

$$\begin{aligned} E_{-n}^{t\theta} &= E_n^{t\theta} \\ E_{-n}^{\phi\theta} &= -E_n^{\phi\theta} \end{aligned} \qquad \text{(A-76)}$$

for a θ polarized incident field and

$$\begin{aligned} E_{-n}^{t\phi} &= -E_n^{t\phi} \\ E_{-n}^{\phi\phi} &= E_n^{\phi\phi} \end{aligned} \qquad \text{(A-77)}$$

for a ϕ polarized incident field. Equations (A-74), (A-76), and (A-77) yield

$$\tilde{E}^s = (E_0^{t\theta} + \sum_{n=1}^{\infty} E_n^{t\theta}\, 2\cos n\phi)\hat{t} + \sum_{n=1}^{\infty} E_n^{\phi\theta}\, 2j \sin n\phi\, \hat{\phi} \qquad \text{(A-78)}$$

for a θ polarized incident field and

$$\underset{\sim}{E}^s = \sum_{n=1}^{\infty} E_n^{t\phi}\, 2j \sin n\phi\, \hat{t} + (E_0^{\phi\phi} + \sum_{n=1}^{\infty} 2 \cos n\phi)\hat{\phi} \qquad \text{(A-79)}$$

for a ϕ polarized incident field.

5. NEAR H-FIELD

Near H-fields (radiated by the BOR electric surface current) are computed in a manner analogous to that for E-fields. Again, reciprocity is employed in the derivation and the test current (now magnetic rather than electric) is given the same "triangular" t variation (A-62). A simpler t variation, such as pulse, could have been chosen for computing the H-fields since derivatives of the test current then do not occur; however, the choice of triangular variation maintains a consistency throughout the overall analysis. The H-field derivation, and computer programming, then can follow closely the H-field development of Mautz and Harrington [1].

The test surface, $\bar{S}$, of Figure A-8 now contains a magnetic surface current, $\underset{\sim}{M}_n$, having $e^{-jn\phi}$ circumferential variation. By reciprocity, [7]

$$-\iint_{\bar{S}} \underset{\sim}{H}_n(\underset{\sim}{J}_n)\cdot\underset{\sim}{M}_n \, ds = \iint_{S} \underset{\sim}{\bar{E}}_n(\underset{\sim}{M}_n)\cdot\underset{\sim}{J}_n \, ds \tag{A-80}$$

where $\underset{\sim}{\bar{E}}_n$ now is the E-field radiated by $\underset{\sim}{M}_n$, $\underset{\sim}{J}_n$ is the n^{th} mode surface current on S, and $\underset{\sim}{H}_n$ is the magnetic field radiated by $\underset{\sim}{J}_n$. From [1 (Section III)]

$$\underset{\sim}{\bar{E}}_n(\underset{\sim}{M}_n) = -\nabla \times \frac{1}{4\pi} \iint_{\bar{S}} \frac{\underset{\sim}{M}_n(\underset{\sim}{r}') \, e^{-jk|\underset{\sim}{r}-\underset{\sim}{r}'|}}{|\underset{\sim}{r}-\underset{\sim}{r}'|} \, ds' \tag{A-81}$$

$$= \frac{1}{4\pi} \iint_{\bar{S}} \frac{1+jk|\underset{\sim}{r}-\underset{\sim}{r}'|}{|\underset{\sim}{r}-\underset{\sim}{r}'|^3} \, e^{-jk|\underset{\sim}{r}-\underset{\sim}{r}'|} \, (\underset{\sim}{r}-\underset{\sim}{r}') \times \underset{\sim}{M}_n(\underset{\sim}{r}') \, ds$$

where $\underset{\sim}{r}$ is a field point at which $\underset{\sim}{\bar{E}}_n$ is evaluated and $\underset{\sim}{r}'$ is a source point (on $\bar{S}$) at which $\underset{\sim}{M}_n$ is evaluated. Primes denote source coordinates and vectors. Then,

$$\underset{\sim}{M}_n = M_n^t \, \hat{t}' + M_n^\phi \, \hat{\phi}' \tag{A-82}$$

and

$$(\underset{\sim}{r}-\underset{\sim}{r}') \times \underset{\sim}{M}_n(\underset{\sim}{r}') = (\underset{\sim}{r}-\underset{\sim}{r}') \times \hat{t}' \, M_n^t(t',\phi') + (\underset{\sim}{r}-\underset{\sim}{r}') \times \hat{\phi}' M_n^\phi(t',\phi') \tag{A-83}$$

The cross products on the right-hand side of (A-83) are evaluated by expressing all vectors in terms of unit vectors $\hat{\rho}$, $\hat{\phi}$, and $\hat{z}$ in the ρ, ϕ, and z directions, respectively.

$$\underset{\sim}{r} = \hat{\rho}\rho + \hat{z}z \tag{A-84}$$

$$\underset{\sim}{r}' = \hat{\rho}\rho' \cos(\phi'-\phi) + \hat{\phi}\rho' \sin(\phi'-\phi) + \hat{z}z' \tag{A-85}$$

$$\hat{t}' = \hat{\rho} \sin v' \cos(\phi'-\phi) + \hat{\phi} \sin v' \sin(\phi'-\phi) + \hat{z} \cos v' \tag{A-86}$$

$$\hat{\phi}' = -\hat{\rho} \sin(\phi' - \phi) + \hat{\phi} \cos(\phi'-\phi) \tag{A-87}$$

Equation (A-85) has been obtained by first writing

$$\underset{\sim}{r}' = \hat{\rho}'\rho' + \hat{z}z' \tag{A-88}$$

and then using Figure A-6 to express $\hat{\rho}'$ in terms of $\hat{\rho}$ and $\hat{\phi}$. To verify (A-86), use Figure A-7 to express $\hat{t}'$ in terms of $\hat{\rho}'$ and $\hat{z}$ and then use Figure A-6 to express ρ' in terms of $\hat{\rho}$ and $\hat{\phi}$.

Substitution of (A-84) through (A-87) into (A-83) yields

$$\begin{aligned}(\underset{\sim}{r}-\underset{\sim}{r}') \times \underset{\sim}{M}_n(\underset{\sim}{r}') = \{&\hat{\rho}\,(-\rho' \cos v' + (z'-z) \sin v') \sin(\phi'-\phi) \\ &+ \hat{\phi}\,(-(\rho-\rho' \cos(\phi'-\phi)) \cos v' - (z'-z) \sin v' \cos(\phi'-\phi)) \\ &+ \hat{z}\rho \sin v' \sin(\phi'-\phi)\}\, M_n^t(t',\phi') + \{\hat{\rho}\,(z'-z) \cos(\phi'-\phi) \\ &+ \hat{\phi}\,(z'-z) \sin(\phi'-\phi) + \hat{z}(-\rho' + \rho \cos(\phi'-\phi))\}\, M_n^\phi(t',\phi')\end{aligned} \tag{A-89}$$

Let v be the angle between $\hat{t}$ and the z axis. v is positive if $\hat{t}$ points away from the z axis and negative if $\hat{t}$ points toward the z axis. Then

$$\hat{t} = \hat{\rho} \sin v + \hat{z} \cos v \tag{A-90}$$

and the $\hat{t}$ and $\hat{\phi}$ components of (A-89) become

$$\hat{t}\cdot[(\underset{\sim}{r}-\underset{\sim}{r}') \times \underset{\sim}{M}_n(\underset{\sim}{r}')] = -(\rho' \sin v \cos v' - \rho \sin v' \cos v$$

$$- (z'-z) \sin v \sin v') \sin (\phi'-\phi) M_n^t(t',\phi') - \{((\rho'-\rho) \cos v \qquad \text{(A-91)}$$

$$- (z'-z) \sin v) \cos (\phi'-\phi) + 2\rho' \cos v \sin^2 (\tfrac{\phi'-\phi}{2})\} M_n^\phi(t',\phi')$$

$$\hat{\phi}\cdot[(\underset{\sim}{r}-\underset{\sim}{r}') \times \underset{\sim}{M}_n(\underset{\sim}{r}')] = \{((\rho'-\rho) \cos v' - (z'-z) \sin v') \cos (\phi'-\phi) \qquad \text{(A-92)}$$

$$- 2\rho \cos v' \sin^2 (\tfrac{\phi'-\phi}{2})\} M_n^t(t',\phi') + (z'-z) \sin (\phi'-\phi) M_n^\phi(t',\phi')$$

The distance $|\underset{\sim}{r}-\underset{\sim}{r}'|$ appearing in (A-81) is the square root of the sum of the squares of $(z-z')$ and the projection of $(\underset{\sim}{r}-\underset{\sim}{r}')$ in the xy plane. Hence,

$$|\underset{\sim}{r}-\underset{\sim}{r}'| = \sqrt{(z-z')^2 + \rho'^2 + \rho^2 - 2\rho\rho' \cos (\phi'-\phi)}$$

$$= \sqrt{(\rho-\rho')^2 + (z-z')^2 + 4\rho\rho' \sin^2 (\tfrac{\phi'-\phi}{2})} \qquad \text{(A-93)}$$

An integral with respect to ϕ' results when the surface integral in (A-81) is iterated. Because this integral with respect to ϕ' is an integral of a 2π periodic function of ϕ' over the period 2π, ϕ' may be replaced by $\phi' + \phi$ without changing the value of the integral. Substitution of (A-91) through (A-93) into (A-81) yields

$$\bar{E}_n(M_n) = \hat{t}\left\{-\frac{k^3}{4\pi}\int\rho'\,dt'\int_0^{2\pi} d\phi'\; GM_n^t(t',\phi'+\phi)\;(\rho'\sin v\cos v' - \rho\sin v'\cos v\right.$$

$$\left.-(z'-z)\sin v\sin v')\sin\phi' - \frac{k^3}{4\pi}\int\rho'\,dt'\int_0^{2\pi} d\phi'\; GM_n^{\phi}(t',\phi'+\phi)\right.$$

$$\left.[((\rho'-\rho)\cos v - (z'-z)\sin v)\cos\phi' + 2\rho'\cos v\sin^2(\tfrac{\phi'}{2})]\right\}$$

$$+\;\hat{\phi}\left\{\frac{k^3}{4\pi}\int\rho'\,dt'\int_0^{2\pi} d\phi'\; GM_n^t(t',\phi'+\phi)\;[((\rho'-\rho)\cos v' - (z'-z)\sin v')\right. \tag{A-94}$$

$$\left.\cos\phi' - 2\rho\cos v'\sin^2(\tfrac{\phi'}{2})]\right.$$

$$\left.+\;\frac{k^3}{4\pi}\int\rho'\,dt'\int_0^{2\pi} d\phi'\; GM_n^{\phi}(t',\phi'+\phi)\;(z'-z)\sin\phi'\right\}$$

where

$$G = \frac{1 + jkR}{k^3R^3}\,e^{-jkR} \tag{A-95}$$

$$R = \sqrt{(\rho-\rho')^2 + (z-z')^2 + 4\rho\rho'\sin^2(\tfrac{\phi'}{2})} \tag{A-96}$$

All the iterated integrals in (A-94) converge because the integrands are at least as well behaved as R^{-1}.

Let

$$\underset{\sim}{M}_n(\underset{\sim}{r}') = \underset{\sim}{M}_n^t(t',\phi') \text{ or } \underset{\sim}{M}_n^{\phi}(t',\phi')$$

where

$$\underset{\sim}{M}_n^t = \hat{t}\ \bar{f}(t')\ e^{-jn\phi'}$$

$$\underset{\sim}{M}_n^\phi = \hat{\phi}\ \bar{f}(t')\ e^{-jn\phi'} \tag{A-97}$$

and $\rho\bar{f}$ is the "triangle" function of Figure A-9. With $\underset{\sim}{J}_n$ given by the n^{th} mode terms in the summation (A-8), the right-hand side of (A-80) becomes

$$\iint_S \underset{\sim}{\bar{E}}_n(\underset{\sim}{M}_n^a)\cdot\underset{\sim}{J}_n\, ds = \tilde{U}_n^{at}\ \vec{I}_n^t + \tilde{U}_n^{a\phi}\ \vec{I}_n^\phi \tag{A-98}$$

where a = t or ϕ, $\vec{I}_n^t$ and $\vec{I}_n^\phi$ are defined following (A-12), and $\tilde{U}_n^{at}$ and $\tilde{U}_n^{a\phi}$ are matrix row vectors. The i^{th} elements of $\tilde{U}_n^{at}$ and $\tilde{U}_n^{a\phi}$ are

$$U_{ni}^{tt} = -jk^3 \int dt\,\rho\, f_i^t(t) \int dt'\ \rho'\,\bar{f}(t')\ (\rho' \sin v \cos v' - \rho \sin v' \cos v$$

$$- (z'-z) \sin v \sin v')\ G_3 \tag{A-99}$$

$$U_{ni}^{t\phi} = k^3 \int dt\,\rho\, f_i^\phi(t) \int dt'\ \rho'\bar{f}(t')\ [((\rho'-\rho) \cos v'$$

$$- (z'-z) \sin v')\ G_2 - G_1\ \rho \cos v'] \tag{A-100}$$

$$U_{ni}^{\phi t} = k^3 \int dt\ \rho\ f_i^\phi(t) \int dt'\ \rho'\bar{f}(t')\ [((\rho'-\rho) \cos v$$

$$- (z'-z) \sin v)\ G_2 + G_1\rho' \cos v] \tag{A-101}$$

$$U_{ni}^{\phi\phi} = jk^3 \int dt\ \rho\ f_i^\phi(t) \int dt'\ \rho'\bar{f}(t')\ (z'-z)\ G_3 \tag{A-10}$$

where

$$G_1 = 2 \int_0^{\pi} d\phi' \; G \sin^2 (\phi'/2) \cos (n\phi') \tag{A-103}$$

$$G_2 = \int_0^{\pi} d\phi' \; G \cos \phi' \cos (n\phi') \tag{A-104}$$

$$G_3 = - \int_0^{\pi} d\phi' \; G \sin \phi' \sin (n\phi') \tag{A-105}$$

The four-impulse approximations (A-31), (A-32), and (A-62) for $\rho f_i^t(t)$, $\rho f_i^{\phi}(t)$, and $\rho' \bar{f}(t')$ reduce (A-99) through (A-102) to

$$\begin{aligned}
U_{ni}^{tt} &= \sum_{p=1}^{4} T_{p+4i-4} \sum_{q=1}^{4} \bar{T}_q \, \bar{U}_s^{tt} \\
U_{ni}^{t\phi} &= \sum_{p=1}^{4} TR_{p+4i-4} \sum_{q=1}^{4} \bar{T}_q \, \bar{U}_s^{t\phi} \\
U_{ni}^{\phi t} &= \sum_{p=1}^{4} T_{p+4i-4} \sum_{q=1}^{4} \bar{T}_q \, \bar{U}_s^{\phi t} \\
U_{ni}^{\phi\phi} &= \sum_{p=1}^{4} TR_{p+4i-4} \sum_{q=1}^{4} \bar{T}_q \, \bar{U}_s^{\phi\phi}
\end{aligned} \tag{A-106}$$

where s denotes the double subscript p+2i-2,q and

$$\bar{U}_{ij}^{tt} = -jk(\bar{\rho}_j \sin v_i \cos \bar{v} - \rho_i \sin v \cos v_i - (\bar{z}_j - z_i) \sin \bar{v}_i \sin \bar{v}) G_3 \tag{A-107}$$

$$\bar{U}_{ij}^{t\phi} = k((\bar{\rho}_j - \rho_i) \cos \bar{v} - (\bar{z}_j - z_i) \sin \bar{v}) G_2 - k\rho_i G_1 \cos \bar{v} \tag{A-108}$$

$$\bar{U}_{ij}^{\phi t} = -(k((\bar{\rho}_j-\rho_i)\cos v_i - (\bar{z}_j-z_i)\sin v_i)G_2 + k\bar{\rho}_j G_1 \cos v_i) \quad \text{(A-109)}$$

$$\bar{U}_{ij}^{\phi\phi} = jk(\bar{z}_j - z_i)G_3 \quad \text{(A-110)}$$

v_i is the angle between the approximate BOR generating curve at (ρ_i, z_i) and the z axis, $\bar{v}$ is the angle between the t coordinate of the test surface and the z axis, and $\bar{\rho}_j$, $\bar{z}_j$ are the ρ, z coordinates of $\bar{t}_j$ in Figure A-9. G_1, G_2, and G_3 are given by (A-103), (A-104), and (A-105) in which G is given by (A-95) with R of (A-96) evaluated at $(\rho, z, \rho', z') = (\rho_i, z_i, \bar{\rho}_j, \bar{z}_j)$.

Due to the rotational symmetry, the $e^{jn\phi}$ variation of $\underset{\sim}{J}_n$ (equation (A-9)) implies the same $e^{jn\phi}$ variation of $\underset{\sim}{H}_n(\underset{\sim}{J}_n)$; i.e., $\underset{\sim}{H}_n(\underset{\sim}{J}_n)$ is expressed by

$$\underset{\sim}{H}_n(\underset{\sim}{J}_n) = \hat{t}\, H_n^t\, e^{jn\phi} + \hat{\phi}\, H_n^{\phi}\, e^{jn\phi} \quad \text{(A-111)}$$

where H_n^t and H_n^{ϕ} are ϕ independent.

If $\underset{\sim}{H}_n$ is approximately uniform over the width of the test surface, $\bar{S}$, and $\underset{\sim}{M}_n$ is given by (A-97), the left-hand side of (A-80) becomes approximately

$$-\iint_{\bar{S}} \underset{\sim}{H}_n(\underset{\sim}{J}_n)\cdot\underset{\sim}{M}_n^a \, ds = -H_n^a \int_0^{4\Delta}\int_0^{2\pi} \bar{f}(t)\,\rho\, d\phi\, dt = -H_n^a\, 4\pi\Delta \quad \text{(A-112)}$$

where a = t or ϕ. Equations (A-80), (A-98), and (A-112) yield

$$H_n^a = \frac{-1}{4\pi\Delta}\,(\tilde{U}_n^{at}\,\vec{I}_n^t + \tilde{U}_n^{a\phi}\,\vec{I}_n^{\phi}) \quad \text{(A-113)}$$

The $\hat{t}$ and $\hat{\phi}$ components of the $\underset{\sim}{H}$-field $\underset{\sim}{H}$ radiated by the BOR surface current are expressed as

$$\hat{t}\cdot\underset{\sim}{H} = H_0^t + \sum_{n=1}^{\infty} (H_n^t\, e^{jn\phi} + H_{-n}^t\, e^{-jn\phi})$$

$$\hat{\phi}\cdot\underset{\sim}{H} = H_0^\phi + \sum_{n=1}^{\infty} (H_n^\phi\, e^{jn\phi} + H_{-n}^\phi\, e^{jn\phi}) \qquad \text{(A-114)}$$

where H_n^t and H_n^ϕ are given by (A-113). As with $\underset{\sim}{E}^s$ of (A-74), the positive and negative "n" modes of $\underset{\sim}{H}$ can be combined, as shown below, for each polarization, θ and ϕ, of incident plane wave (A-1) and (A-2). A second superscript on H_n^t, H_n^ϕ, $\vec{I}_n^t$, or $\vec{I}_n^\phi$ in the following development refers to this incident field polarization.

It is apparent from (A-99) through (A-102) that

$$\tilde{U}_{-n}^{tt} = -\tilde{U}_n^{tt}$$

$$\tilde{U}_{-n}^{t\phi} = \tilde{U}_n^{t\phi} \qquad \text{(A-115)}$$

$$\tilde{U}_{-n}^{\phi t} = \tilde{U}_n^{\phi t}$$

$$\tilde{U}_{-n}^{\phi\phi} = -\tilde{U}_n^{\phi\phi}$$

From (A-113), (A-53), and (A-115), therefore,

$$H_{-n}^{t\theta} = -H_n^{t\theta}$$

$$H_{-n}^{\phi\theta} = H_n^{\phi\theta} \qquad \text{(A-116)}$$

for a θ polarized incident field and

$$H_{-n}^{t\phi} = H_n^{t\phi}$$

$$H_{-n}^{\phi\phi} = -H_n^{\phi\phi} \qquad \text{(A-117)}$$

for a ϕ incident field. Equations (A-114), (A-116), and (A-117) yield

$$\underline{H} = \sum_{n=1}^{\infty} H_n^{t\theta} 2j \sin n\phi \, \hat{t} + (H_0^{\phi\theta} + \sum_{n=1}^{\infty} H_n^{\phi\theta} 2 \cos n\phi)\hat{\phi} \tag{A-118}$$

for a θ polarized incident field and

$$\underline{H} = (H_0^{t\phi} + \sum_{n=1}^{\infty} H_n^{t\phi} 2 \cos n\phi)\hat{t} + \sum_{n=1}^{\infty} H_n^{\phi\phi} 2j \sin n\phi \, \hat{\phi} \tag{A-119}$$

for a ϕ polarized incident field.

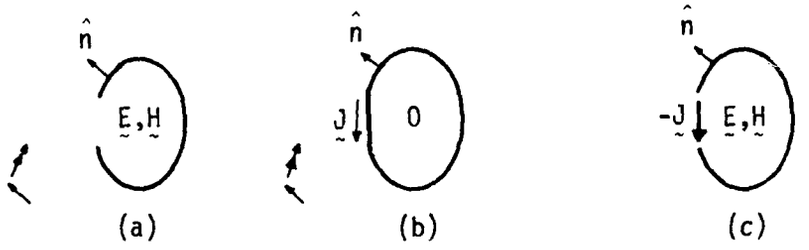

Figure A-10. An Equivalence Theorem

6. APERTURE COUPLING

The method for computing the near scattered fields of a BOR with edges (Sections 1 through 5 of this appendix) is, in theory, directly applicable to computing the fields penetrating a conducting BOR with rotationally symmetric apertures; e.g., Figure A-1. The internal field is the vector addition of the scattered field (Sections 4 and 5) and the impressed field. For plane wave excitation, the impressed field is the incident field $\underset{\sim}{E}^e$ given by either (A-1), (A-2), or a linear combination of (A-1) and (A-2). Each BOR model component of $\underset{\sim}{E}^e$, at a field point of interest, is readily computed from relations similar to those of Section 2.

As often occurs with well-shielded bodies (e.g., those having only tiny or thin apertures), the scattered and impressed fields are nearly equal and opposite at points within the body. The vector sum of these fields then is a subtraction of almost equal numbers with an associated loss of accuracy. This undesirable computation is avoided by invoking an equivalence theorem, due to Schelkunoff [8], whereby the cavity field is computed as a radiation problem once an equivalent aperture excitation is determined. This theorem states that the original problem, containing sources external to the body, can be replaced with an equivalent problem having only aperture current sources for excitation. Figure A-10 illustrates this where the original problem (Figure 10a) is equivalent to the sum of the two problems (Figures 10b and c). The induced surface current $\underset{\sim}{J}$ in the vicinity of the aperture is found for the apertureless (cover aperture with conductor) body in the presence of the external sources (Figure 10b). Then, $(-\underset{\sim}{J})$ becomes an aperture excitation resulting in the external fields of the original problem (Figure 10c). The application of this theorem to the moment method formulation of the BOR aperture coupling problem has been described in [9]. An intermediary aperture tangential $\underset{\sim}{E}$-field computation was employed and the method called BOR3. The method is called the Equivalent Aperture Excitation Technique, EAET, in this report.

A modified method that avoids the aperture field computation has been developed [10]; however, knowledge of the aperture tangential $\underset{\sim}{E}$-field when the aperture is "empty" is useful in incorporating the Aperture Loading Technique, ALT, discussed in the main body of this report. The ALT accounts for odd shaped, material filled, thin apertures such as occurs at "sleeve" type joints between BOR sections. Thus, the following description of EAET is an adaptation of [9] to the development in Sections 1 through 5 of this appendix.

The apertures are removed (covered with perfect conductors). The induced current on this "short-circuited" BOR is expanded as

$$\underset{\sim}{JS} = \sum_{n,j} \left(IS^{t}_{nj} \, \underset{\sim}{J}^{t}_{nj} + IS^{\phi}_{nj} \, \underset{\sim}{J}^{\phi}_{nj} \right) \tag{A-120}$$

where column vectors $\vec{IS}^{t}_{n}$ and $\vec{IS}^{\phi}_{n}$, composed of the coefficients IS^{t}_{nj} and IS^{ϕ}_{nj}, respectively, are the solutions $\vec{I}^{t}_{n}$ and $\vec{I}^{\phi}_{n}$ of (A-20).

The apertures are replaced (shorting conductors removed) and are filled with the equivalent aperture current source, $\underset{\sim}{JA}$, expanded as

$$\underset{\sim}{JA} = \sum_{n,p} \left(IA^{t}_{np} \, \underset{\sim}{J}^{t}_{nj_p} + IA^{\phi}_{np} \, \underset{\sim}{J}^{\phi}_{nj_p} \right) \tag{A-121}$$

where

$$\begin{aligned} IA^{t}_{np} &= - IS^{t}_{nj_p} \\ IA^{\phi}_{np} &= - IS^{\phi}_{nj_p} \end{aligned} \tag{A-122}$$

and the p^{th} t-directed (or ϕ-directed) aperture expansion function is the $j_p{}^{th}$ corresponding generating curve expansion function. The external incident field, $\underset{\sim}{E}^{e}$, is removed and this new problem analyzed as follows. First, the aperture tangential component of $\underset{\sim}{E}$-field is expanded as

$$\underset{\sim}{EA}_{tan} = \sum_{n,p} \left(EA^{t}_{np} \, \hat{t} + EA^{\phi}_{np} \, \hat{\phi} \right) \tag{A-123}$$

where

$$\begin{aligned} EA^{t}_{np} &= - VA^{t}_{np} \, \delta(t - t^{-}_{2j_p+1}) \frac{e^{jn\phi}}{2\pi} \\ EA^{\phi}_{np} &= - VA^{\phi}_{np} \, \delta(t - t^{-}_{2j_p+1}) \frac{e^{jn\phi}}{2\pi} \end{aligned} \tag{A-124}$$

$\delta(t)$ (Section 1 of this appendix) denotes the unit impulse function, and $t^{-}_{2j_p+1}$ (Figure A-3) is the BOR generating curve t coordinate of the triangle function

$\rho f^{t}_{j_p}(t)$ (or $\rho f^{\phi}_{jp}(t)$)peak. The j_p^{th} generating curve triangle function is the p^{th} aperture located triangle function.

Each VA^{t}_{np} and VA^{ϕ}_{np} can be thought of as port voltage sources through which a surface current flows. One seeks values of VA^{t}_{np} and VA^{ϕ}_{np} for which JA, given by (A-121) and (A-122), flows through the aperture ports. These values are obtained by relating the IA^{t}_{np} and IA^{ϕ}_{np} of (A-121) to the VA^{t}_{np} and VA^{ϕ}_{np} by the matrix equation

$$\begin{bmatrix} \vec{IA}^{t}_{n} \\ \vec{IA}^{\phi}_{n} \end{bmatrix} = \begin{bmatrix} [YA^{tt}_{n}] & [YA^{t\phi}_{n}] \\ [YA^{\phi t}_{n}] & [YA^{\phi\phi}_{n}] \end{bmatrix} \begin{bmatrix} \vec{VA}^{t}_{n} \\ \vec{VA}^{\phi}_{n} \end{bmatrix} \qquad \text{(A-125)}$$

and solving (A-125). In (A-125), the p^{th} elements of $\vec{IA}^{t}_{n}$, $\vec{IA}^{\phi}_{n}$, $\vec{VA}^{t}_{n}$, and VA^{ϕ}_{n} are IA^{t}_{np}, IA^{ϕ}_{np}, VA^{t}_{np}, and VA^{ϕ}_{np}, respectively. The matrix of $[YA^{ab}_{n}]$, ab = tt, ϕt, tϕ, and $\phi\phi$ submatrices is called the "aperture admittance matrix."

The pq^{th} elements of $[YA^{ab}_{n}]$, ab = tt, ϕt, tϕ, and $\phi\phi$, are found by "exciting" the BOR with the tangential aperture field, $\underset{\sim}{EA}_{tan}$, given by (A-123). This requires satisying the boundary condition

$$\underset{\sim}{E}^{s}_{tan} = \underset{\sim}{EA}_{tan} \qquad \text{on S} \qquad \text{(A-126)}$$

where (Section 1 of this appendix) $\underset{\sim}{E}^{s}$ is the field radiated by the BOR surface current, $\underset{\sim}{J}$. A development similar to that following (A-3) applied to (A-126) yields (A-20) with the exception that the j^{th} element of $\vec{V}^{t}_{n}$ and V^{ϕ}_{n} are, respectively,

$$V^{t}_{nj} = \begin{cases} VA^{t}_{np} & j = j_p \\ 0 & \text{otherwise} \end{cases}$$

$$V^{\phi}_{nj} = \begin{cases} VA^{\phi}_{np} & j = j_p \\ 0 & \text{otherwise} \end{cases} \qquad \text{(A-127)}$$

The elements of $\vec{I}_n^t$ and $\vec{I}_n^\phi$ in (A-20) corresponding to aperture expansion functions are the elements of $\vec{IA}_n^t$ and $\vec{IA}_n^\phi$; i.e.,

$$I_{nj}^t = IA_{np}^t \qquad \text{if } j = j_p$$

$$I_{nj}^\phi = IA_{np}^\phi \qquad \text{if } j = j_p \tag{A-128}$$

In light of (A-125), (A-127), and (A-128) and defining the inverse of the impedance matrix in (A-20) as

$$\begin{bmatrix} [Y_n^{tt}] & [Y_n^{t\phi}] \\ [Y_n^{\phi t}] & [Y_n^{\phi\phi}] \end{bmatrix} = \begin{bmatrix} [Z_n^{tt}] & [Z_n^{t\phi}] \\ [Z_n^{\phi t}] & [Z_n^{\phi\phi}] \end{bmatrix}^{-1} \tag{A-129}$$

the pq^{th} elements of $[YA_n^{tt}]$, $[YA_n^{\phi t}]$, $[YA_n^{t\phi}]$, and $[YA_n^{\phi\phi}]$ become

$$\begin{aligned} YA_{npq}^{tt} &= Y_{nj_pj_q}^{tt} \\ YA_{npq}^{\phi t} &= Y_{nj_pj_q}^{\phi t} \\ YA_{npq}^{t\phi} &= Y_{nj_pj_q}^{t\phi} \\ YA_{npq}^{\phi\phi} &= Y_{nj_pj_q}^{\phi\phi} \end{aligned} \tag{A-130}$$

The solution of (A-125), with $\vec{IA}_n^t$ and $\vec{IA}_n^\phi$ given by (A-122), provides the aperture port voltage sources that correspond to the aperture tangential $\underset{\sim}{E}$-field within the approximation (A-124). Excitation of the BOR with these voltage sources yields the

internal fields of the original problem. This final analysis is carried out by solving (A-20) for the BOR surface current coefficients with $\vec{V}_n^t$ and $\vec{V}_n^\phi$ given by (A-127). These current coefficients then are used to determine the near $\underline{E}$- and $\underline{H}$-fields as detailed in Sections 4 and 5 of this appendix.